2019-12-01

Variance Reduction in Wind Farm Layout Optimization

Bertelsen Gagakuma
Brigham Young University

Variance Reduction in Wind Farm Layout Optimization

Bertelsen Gagakuma

A thesis submitted to the faculty of
Brigham Young University
in partial fulfillment of the requirements for the degree of

Master of Science

Andrew Ning, Chair
Julie Crockett
Steve E. Gorrell

Department of Mechanical Engineering

Brigham Young University

ABSTRACT

Variance Reduction in Wind Farm Layout Optimization

Bertelsen Gagakuma
Department of Mechanical Engineering, BYU
Master of Science

As demand for wind power continues to grow, it is becoming increasingly important to minimize the risk, characterized by the variance, that is associated with long-term power forecasts. This thesis investigated variance reduction in power forecasts from wind farm layout optimization. The problem was formulated as a multi-objective optimization one of maximizing mean-plant-power and minimizing variance. The $\varepsilon-$constraint method was used to solve the bi-objective problem in a two-step optimization framework where two sequential optimizations are performed. The first is maximizing mean wind farm power alone and the second, minimizing variance with a constraint on the mean power which is the value from the first optimization. The results show that the variance in power estimates can be reduced by up to 30%, without sacrificing mean plant power for the different farm sizes and wind conditions studied. This reduction is attributed to the multi-modality of the design space which allows for unique solutions of high mean plant power at different power variances. Thus, wind farms can be designed to maximize power capture with greater confidence.

Keywords: mean plant/farm power, variance reduction, wind farm layout, optimization, multi-modality

ACKNOWLEDGMENTS

My sincerest gratitude goes to my advisor Dr. Ning of the Mechanical Engineering Department at Brigham Young University. I am thankful and indebted to him for sharing his expertise, and extending to me his the valuable guidance and encouragement. He consistently allowed this paper to be my own work, but steered me in the right direction whenever he thought I needed it.

I take this opportunity to as well express appreciation to all of the members of the BYU FLOW lab for their help and support throughout the years; particularly P.J. Stanley. Without his passionate participation and input, this research could not have been successfully conducted.

Finally, I must express my very profound gratitude to my family for providing me with unfailing support and continuous encouragement throughout my years of study and through the process of researching. This accomplishment would not have been possible without them. Thank you.

TABLE OF CONTENTS

LIST OF TABLES

LIST OF FIGURES

NOMENCLATURE

A	Wind turbine rotor swept area
A_q^{OL}	Wake overlap area in FLOIRS wake model
α	Wind direction
C_p	Wind turbine power coefficient
D	Wind turbine rotor diameter
$D_{w,q}$	Downwind wake diameter in FLORIS wake model
$E[P]$	Expected wind farm power
ε_i	Objective function set as a constraint
$f_{frequency}$	Wind frequency as a function of wind direction
f_{speed}	Wind speed as a function of wind direction
$f(\mathbf{x})$	Generic objective function of $\mathbf{x}$
μ_p	Mean-plant-power
μ_P^*	Mean-plant-power from phase 1 optimization
$n_{samples}$	Number of samples in Monte Carlo intergration
n_{turbs}	Number of wind turbines
P	Total wind farm power
P_i	Power contribution from a single turbine
$\phi(\alpha)$	Wind direction probability density function
ρ	Air density
$S_{i,j}$	Turbine spacing
σ_1^2	Variance from phase 1 optimization
σ_2^2	Variance from phase 2 optimization
σ^2	Variance in Monte Carlo integration
σ_P^2	Variance in power production
U	Turbine hub wind speed
V	Free stream velocity
x	Turbine *'x'* location within farm boundaries
$\mathbf{x}$	Generic vector of design variables
y	Turbine *'y'* location within farm boundaries

CHAPTER 1. INTRODUCTION

1.1 Brief History of Wind Power

Wind, one of the earliest forms of energy, has been harnessed by man throughout the ages. Boats were powered by wind energy as early as 5000 BC along the Nile. Other notable initial applications of wind energy include its use for grain milling and water pumping in Persia and China between 500 and 900 BC[1]. In later centuries, wind power technology (with complex mechanical systems) received much attention around AD 1000 in Europe where it was used in water pumping projects in the Netherlands. As demand for electricity begun to increase during the industrial revolution, wind power technology was also considered for electricity generation. The first known electricity generating wind turbine was built in 1887 by James Blyth in Scotland[2]. Poul la Cour, Joe and Marcellus Jacobs, Johannes Juul continued to develop the technology for harnessing wind power for and electricity production all through the early 1900s. The second world war brought many technological advancements in aerospace and other areas. During this era, a 1.25 MW wind turbine was used to power a local community for months in Vermont. Thus wind had become a well proven source of electric power generation by this time. However, hydroelectric power and fossil fuels were mainly used for power generation in those days.

But the 1970s brought some hope for hope for wind, and rewables in general as petroleum prices begun to rapidly increase. In the United States, there was increasing interest in alternative forms of power generation. There was also a push for cleaner energy in Europe during that period because of an increasing awareness of the harmful environmental impacts of fossil fuels. The potential of wind power as a viable source of electricity was subsequently exploited on both continents leading to the establishment of the first commercial wind farms in California and Denmark.

[1] https://www.renewableenergyworld.com/ugc/articles/2014/11/history-of-wind-turbines.html
[2] https://blogs.bl.uk/science/2017/08/james-blyth-and-the-worlds-first-wind-powered-generator.html

The lessons learned from those implementations paved the way for most of the technologies and methods used in wind power generation to date.

The 1990s, however, saw stable oil prices, hence a decline in interest for renewable energy sources. Furthermore, large wind power projects had a few drawbacks such as high capital costs, limited ancillary technology, and the sporadic nature of wind resources. Some of these downsides still exist today, and rendered wind energy undesirable for a time. But a recent global push towards clean energy has made a case for wind once again. Modern technologies (faster computers, weather satellites, more reliable materials, etc.) are now making wind a competitive renewable energy option.

1.2 Wind Energy Today

Wind is a feasible source of power generation these days. Commercial wind turbines generated almost 4% of world electricity in 2018[3]. This was the highest contribution from renewables (besides hydro power) in that year. The global installed wind power capacity has also steadily increased since the mid 1990s (Figure 1.1), and it is worth pointing out that wind has become one of the fastest-growing sources of electricity. Industry experts now believe that wind promises to be a viable and sustainable source of energy. This positive press for wind has prompted the U.S Department of Energy (DOE) to research the possible benefits of future wind energy projects. The DOE estimates that total wind power by the year 2050 will reach 404.25 GW nationwide[4]. This is about 38% of the current total installed electricity generation capacity in the country.

This potential to increase installed wind energy capacity is due to many factors, including technological advancements, policy initiatives, and economic drivers that are now making wind energy a cost-competitive option to world energy demands. We now see an ever growing support for wind and other green sources by many of the world's governments who aim to meet cleaner emissions standards in combating climate change. Although western European countries and the United States have dominated the wind energy scene for years, the last decade has introduced new

[3]https://www.iea.org/topics/renewables/wind/

[4]https://www.energy.gov/maps/map-projected-growth-wind-industry-now-until-2050

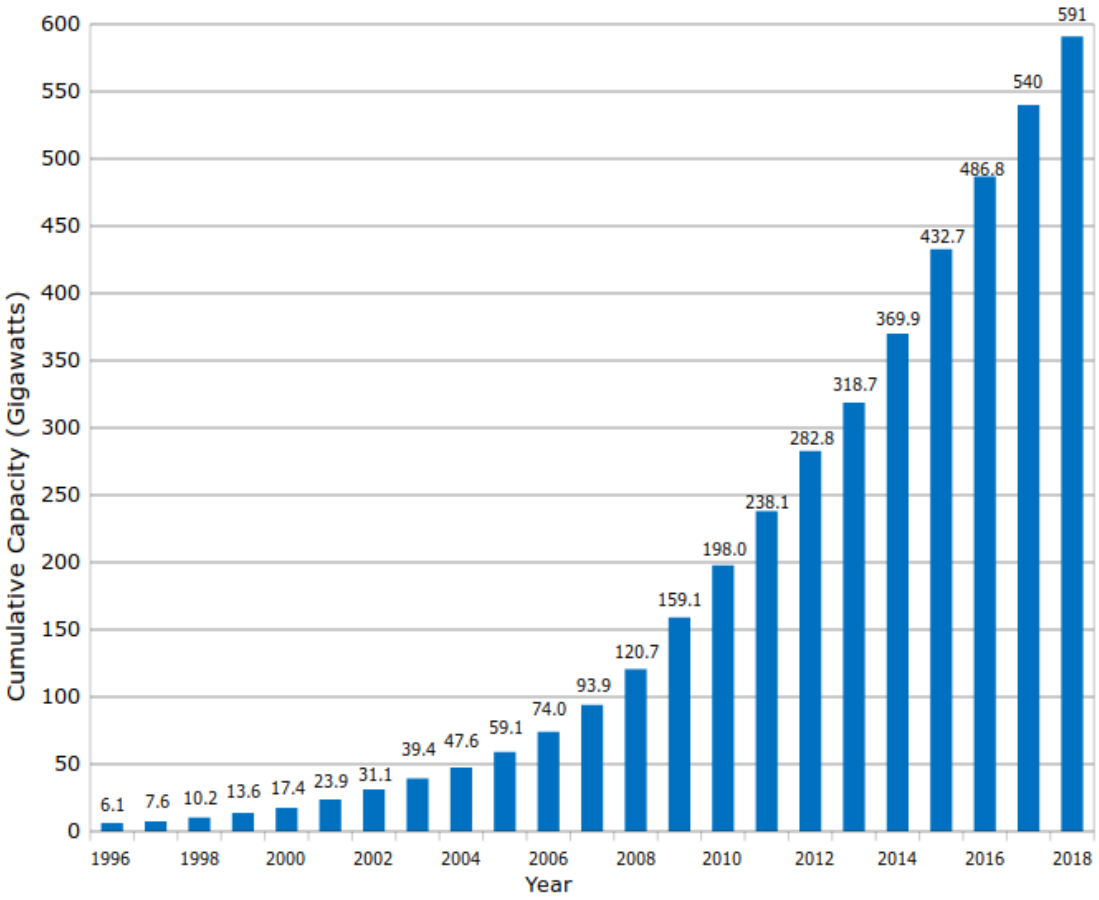

Figure 1.1: Global cumulative installed wind capacity in gigawatts from 1996 - 2017[5].

players in Asia, and Latin America. Worth mentioning is China, where in 2015 they installed more wind turbines than in the European Union in that period[6].

As previously mentioned, the main factors that affect the cost of wind energy are initial capital costs, variable wind conditions, and operating costs [1]. Because these factors are inherently stochastic, they require special statistical and computational techniques for proper characterization during wind farm modelling. Thus scientists, engineers, and economic planners all play major roles in developing wind projects. On the engineering side of things, computational fluid dynamics (CFD) is a high fidelity analytic tool for accurately treating fluid flows, but its slow speed and intense computer hardware demands has prompted others to devise more efficient ways of mod-

[5]Global Wind Power Cumulative Capacity graph from Wikimedia Commons (https://commons.wikimedia.org/wiki/File:Global_Wind_Power_Cumulative_Capacity.svg#filelink), by Delphi234, Data: GWEC.

[6]https://www.gwec.net/wp-content/uploads/vip/GWEC-Global-Wind-2015-Report_April-2016_22_04.pdf

eling flows in wind farms. Research into such methods is on the rise in many universities and government research labs around the world. These works revolve around the development of so called engineering wake models, and other methods for determining turbine hub velocities. This area of research has particularly received much attention in recent times, building on the works of N.O. Jensen and others [2–5].

Although there have been many technological advances in recent times that have made wind energy more favorable, it remains an intermittent energy source, marked by high variability in power generation. This variability is mainly attributed to meteorological fluctuations, and can be classified as either short-term, or long-term.

Short-term variability includes minute-to-minute, hour-to-hour (Figure 1.2), and day-to-day fluctuations in power production which are consequences of turbulence and transient events. This form of variability can be predicted fairly easily. Quantifying short-term variability is crucial for grid management and electricity pricing [6, 7]. It can be managed with appropriate load balancing schemes in grid systems that are fed by different electricity sources to meet demand.

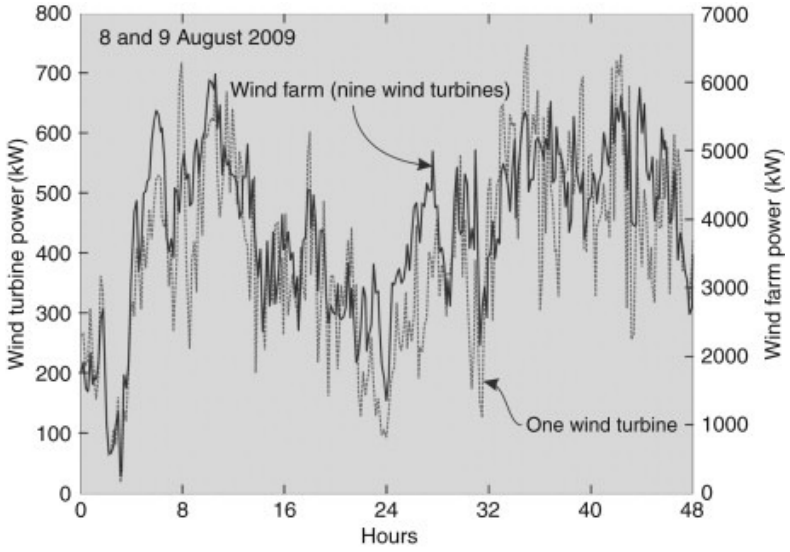

Figure 1.2: Hour-to-hour fluctuations in power production.[7]

Long-term variability on the other hand involves fluctuations over longer periods such as monthly or seasonal time frames, and years. Figure 1.3 shows the monthly average Danish wind

[7]This graph was reprinted from Comprehensive Renewable Energy, J.A. Carta, Chapter: 2.18 Wind Power Integration, Figure 35, Copyright (2012), with permission from Elsevier.

electric power generation with noticeable fluctuations between the years. Long-term variability in wind power output is caused by climate effects, and is not important for the day-to-day operation of wind farms, but as the name suggests is very crucial for long-term project development and maintenance planning [8, 9].

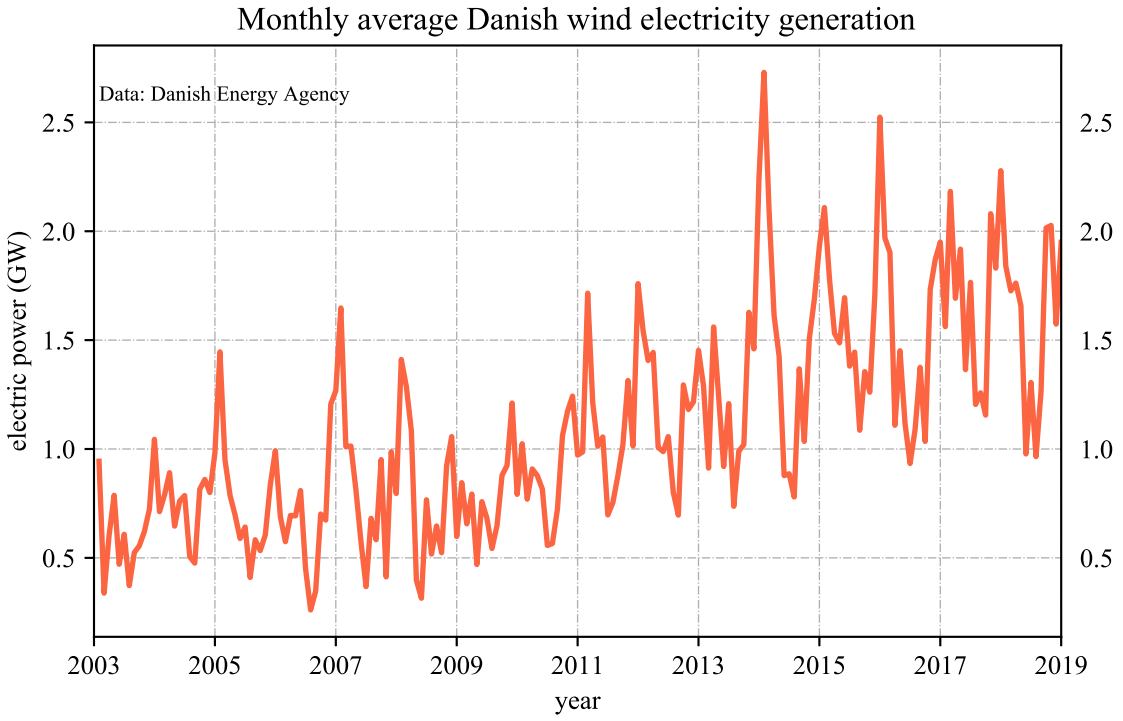

Figure 1.3: Inter-annual variation in Danish power production 2003 - 2019[8].

As wind power continues to grow, and it is not only desirable to increase global wind energy capacity as a clean energy source, but also to minimize the risks associated with long-term power forecasts. Wind energy predictions will, however, be unavoidably subject to epistemic uncertainties due to the inherent randomness in weather and climate conditions. But it is instructive to study the evolution of key statistical quantities such as variance and different percentiles in wind farm layout design to help reduce fluctuations in long-term power forecasts. The variance is examined in this work to create designs that are more stable against long-term power production fluctuations. Doing this will allow wind farm operators and economic planners to make more informed decisions [10].

[8]Data from Danish Energy Agency was used to make this graph (https://ens.dk/sites/ens.dk/files/Analyser/grunddata2018_-_basicdata2018.xlsx).

As it is desirable to obtain solutions which are wind farm layout designs with lower risk in power production, the goal of this thesis is to show that one can design wind farm layouts to have lower risk associated with mean power output. Presented here is a two stage process for long-term wind plant power variance reduction in which statistical constraints are integrated into the layout optimization framework to reduce the variance associated with mean power forecasts. The concept is tested on a variety of wind farms with different farm boundaries, wind roses, numbers of turbines, and turbine densities, to search for designs with high power production that are robust against changes in wind direction. The main benefit of the approach is that it requires zero sacrifice in mean plant power production for reducing the variance.

1.3 Wind farm layout optimization

The power generated in a wind farm is strongly dependent on how wind turbines are arranged. For a given site, energy capture can be improved through wind farm layout optimization. This is a critical step in farm design, as wind turbine assemblies (tower, rotor, generator, controls, etc.) are massive systems that typically remain fixed in place for the operational lifetimes of wind farms. Many groups around the world therefore study this problem of optimal turbine positioning by using past wind data for predicting future power production since smart turbine placement favors superior energy capture. The objectives used in wind farm layout optimization include power [11], annual energy production (AEP) [12, 13], net present value (NPV) [14], profit [15, 16], and the cost of energy (COE) [17, 18]. These objectives, defined in Appendix A, are fundamentally functions of the mean farm power output, and therefore do not consider power variance. The mean power output is not the only important objective; for power companies it is important to minimize variability as well since a low variance translates to less deviation from mean power output forecasts over time. Thus, lowering the variance increases the robustness of wind farm power estimates.

The wind farm layout optimization problem is a high dimensional problem in a fundamentally multi-modal design space [19, 20]. This is due to the large number of design variables and the differing wind conditions at wind plant sites. The multi-modality of the design space is an indication that there are many different solutions to the problem, with some solutions showing lower power variance with corresponding high mean power values over others. This characteris-

tic of wind farm layout optimization problems can therefore be exploited to produce more robust wind farm designs against fluctuations in weather conditions even though obtaining solutions in the design space may sometimes be difficult.

Multi-modality in this design space can be addressed using other global search methods [19] or performing optimizations with multiple starting locations. Evolutionary algorithms are, however, computationally expensive, and are not very efficient at handling high dimensional spaces as this. Gradient-based methods on the other hand are very efficient in high dimensional spaces but struggle with multi-modality. One way of getting around these problems is using multiple starting locations with gradient based methods. Doing this brings the best of both worlds, thus offering a good framework for finding optimal solutions in the wind farm layout optimization design space. This work takes advantage of the multi-modality of the design space to reduce the variance associated with long-term power forecasts.

1.4 Variance reduction

Standard variance reduction methods include antithetic sampling, stratification, common random numbers, conditioning and control variates, and importance sampling [21, 22]. These methods incorporate various intelligent sampling schemes and information about solutions to similar problems to improve the efficiency of Monte Carlo methods. This is because the error associated with the variance in Monte Carlo simulations scales inversely with the number of samples ($\varepsilon_{\sigma^2} \propto \sigma^2/n_{samples}$). Thus Monte Carlo simulations require large $n_{samples}$ for improved accuracy in models. But large $n_{samples}$ also implies longer time and huge demands on computer resources [23, 24]. Furthermore, using such variance reduction methods adds complexity to problems, particularly when performing importance sampling and applying conditioning and control variates [22]. More than the added complexity to problems Monte Carlo simulations are generally time intensive processes and are not a very efficient method for performing wind farm layout optimization. Because of these limitations, simpler techniques were applied to reduce the power variance of wind plant power estimates in this work. These techniques involve reducing the variance with multi-objective optimization.

One such approach to reducing the variance in wind farm power predictions is to perform a multi-objective optimization using Pareto optimization. The Pareto approach allows for easy

comparison of different objectives and has been applied to wind farm design. Mytilinou et al. used Pareto analysis to study the trade-off between location, turbine type, and turbine count to suggest optimum regions for siting wind farms around the UK [25]. Their objectives were Life Cycle Cost (LCC), number of turbines, extracted power, and total installed site capacity. Borrisova and Mustakerov also used such methods to test their multi-objective model and algorithm by studying the effects of different combinations of farm location, turbine counts, and wind conditions on cost of energy and power output in wind farm design [26]. Pareto optimization presents a view of the best solutions between competing objectives, and can be used to study the trade-offs between mean power and variance. The approach requires several hundred to thousands of evaluations to effectively provide accurate information. For this reason, Pareto optimization is a time intensive and computationally expensive process for this problem due to the high dimensionality and nonlinearity of the design space. Moreover, it may not always be necessary to obtain all the Pareto optimal solutions to a multi-objective problem as was shown in this work.

Some researchers have also considered and accounted for the uncertainty of wind resources in their procedures for power forecasting. While these efforts are not directly targeted at reducing variance, they improve the accuracy and robustness of wind farm power predictions by more accurately calculating statistics of interest such as mean power and variance. As wind is a stochastic resource, a major part of characterizing uncertainties in wind farm layout design is defining the proper probability density functions for flow conditions. This concept has been used in many wind energy works where researchers create joint probability distributions for the interdependent variables wind speed and direction [27] and use probability density functions for random variables in the design space in polynomial chaos expansions to quantify uncertainties [1, 28]. Such efforts have been largely focused on rightly describing random variables in wind farm layout optimization. By incorporating stochastic elements into the optimization process, researchers are able to predict plant power output more realistically by accurately determining the aforementioned useful statistics. Once the mean power and variance are properly described, further optimizations can be performed to reduce the variance.

One can also perform constrained optimizations to maximize power output and reduce variance in wind farm layout design without developing a full Pareto front. This is similar to the work of Tingey et al. where they explored the trade-offs between reducing noise level and

maximizing power output through wind farm layout optimization for one wind direction [29]. To achieve a good compromise between the two, they enforced an upper limit constraint on the system sound pressure level (SPL) based on appropriate acoustic models to optimize the layouts of two existing wind farms with turbine rotation noise issues. From that analysis, they found that wind farm layouts can be improved to reduced noise levels at very little expense to power output. This concept was used to reduce variance in wind farm layout optimization while keeping mean power constant in this thesis. As a step in further improving accuracy, the problem is rightly treated as a stochastic one here. Thus samples are drawn from probabilistic wind direction distributions to determine the values of key statistical quantities in the wind farm layout optimization schemes.

As mentioned earlier, the wind farm layout optimization problem is one in a highly multi-modal design. Because of this multimodality, multiple layout designs can be obtained that produce nearly identical mean wind power ($\approx$3% of each other) but with variances spread over much wider ranges (up to 30% between extremes). The wide spread suggests that an optimization of the variance could potentially result in layouts that produce high mean power with lower power variance. This characteristic of the wind farm layout design space is extensively explored in this work.

The rest of this thesis is organized as follows: Chapter 2 contains a summary of the models and optimization framework for this problem including wind farm description, flow properties and the FLORIS wake model, statistics of interest, and multi-objective optimization, Chapter 3 presents the results analysis and discussion, and Chapter 4 gives the concluding remarks.

CHAPTER 2. METHODOLOGY

The following is an overview of the different tools and techniques employed in this work, with sections discussing wind farm and flow property modeling, as well as relevant statistical quantities and the optimization framework for this problem.

2.1 Wind Farm Modeling

The 3.35 MW onshore wind turbine developed by the International Energy Agency (IEA)[1] is used in this work. This wind turbine was chosen because it was developed for wind energy research hence there is open-access to all of its specifications. It is comprised of a three-blade rotor, which has a swept diameter of 130 m and a 110 m hub height. The power generator is rated at 3.35 MW with a power conversion efficiency of 93%.

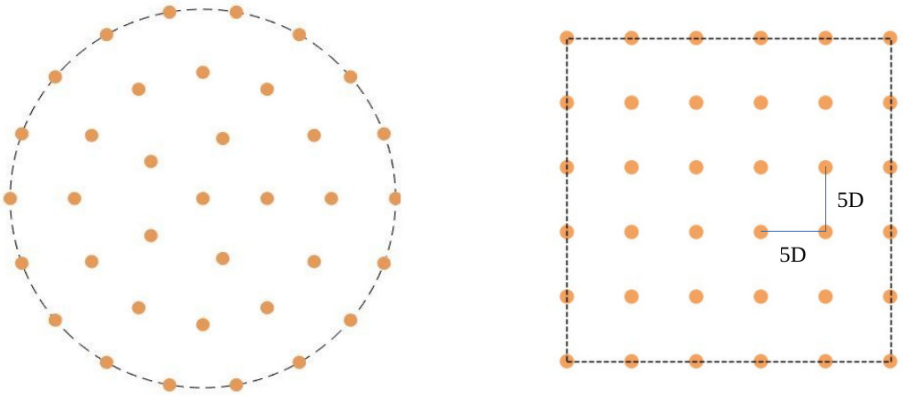

Figure 2.1: 36-turbine circle and square boundary wind farms. The wind farm area is determined by the area required to have the turbines arranged in a perfect square grid with a spacing of five rotor diameters between turbines. Both circle and square boundaries enclose the same area for a given number of turbines.

[1] https://www.nrel.gov/wind/assets/pdfs/se17-9-iea-wind-task-37-systems-engineering.pdf

There were several cases considered in this variance reduction study. A case is made up of a boundary type (circle or square), number of turbines (16, 36, or 64), and wind conditions (from locations in Victorville, Redding, and the Princess Amalia wind farm).

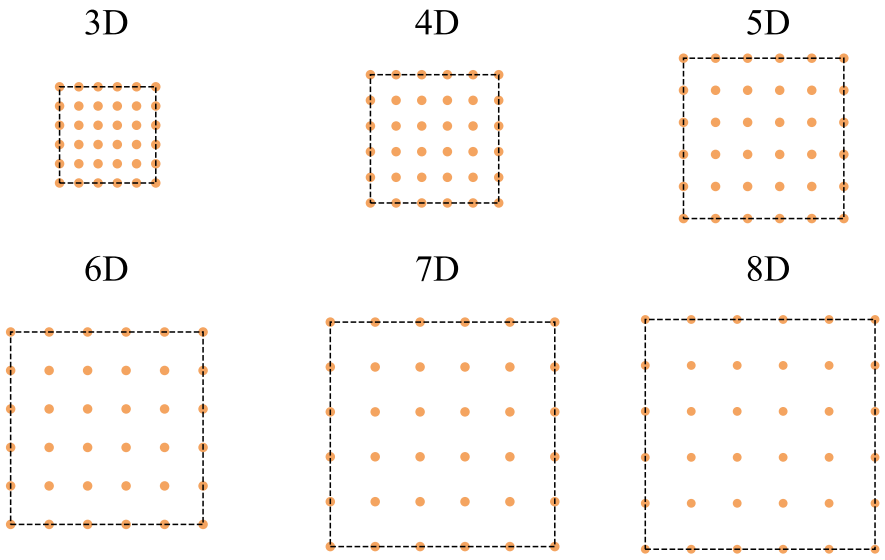

Figure 2.2: 36-turbine square wind farm at six different turbine densities.

The circle and square boundaries (Figure 2.1) have equal areas that depend on the number of turbines under consideration. Although operational wind farms rarely have circle, square, or standard plane geometry boundaries as the ones presented here, these choices are sufficient for proving the intended concepts. With the exception of two cases, the wind farm area is determined by the area required to have the turbines arranged in a perfect square grid with a spacing of five rotor diameters between turbines (as in Figure 2.1 which shows this sort of spacing for 36 turbines in circle and square farm boundaries). The two special cases were performed on 36-turbine circle and square boundary farms with different turbine spacing; cases where the number of turbines is

kept constant and the land area varied, based on different initial rotor diameter spacing. Figure 2.2 shows this sort of case for a 36-turbine square farm at six different turbine densities which are based on turbine spacings of 3 to 8 rotor diameters apart.

Other assumptions made in this analysis are flat terrains in all cases and all turbines are of the same size and characteristics. Also, all wind directions in this work are parallel to the horizontal rotational axis of the wind turbines.

2.2 Wake Model

A consequence of changing wind direction is intermittent rotor waking. Wakes in wind farms are regions downstream of turbines where the wind speed is significantly less than the free stream velocity. This reduction in speed is caused by a loss in the flow energy as upstream turbines extract energy from wind as it flows over turbine blades to generate rotational motion. Each turbine wake can be approximated as a truncated cone starting at the blade tips, and expanding downstream, but also decaying with distance. There are a few notable scenarios of turbine−wake interactions worth considering, namely, 1) a rotor completely in the wake of an upstream turbine, 2) a partially waked rotor, and 3) a rotor affected by multiple wakes (partially or completely). In all of these cases the wind speed across the rotor is lower than the free stream, and therefore translates to lower power production. Wind turbine layouts are therefore arranged in a manner that reduces wake interactions in power production.

Even though CFD is a more accurate method for simulating fluid flows, an engineering wake model is used in this analysis for reasons mentioned in Section 1.2. Engineering wake models are analytical models for describing wakes in wind farms. They are derived from applying fluid conservation laws across a wind turbine's rotor to determine downwind velocity conditions. The wake model used in this work is the Flow Redirection and Induction in Steady-state (FLORIS) engineering wake model [30]. This is a derivative of the Jensen wake model developed by N.O. Jensen [2] which assumes a linearly expanding wake with a velocity deficit that is only dependent on the distance behind a rotor. The FLORIS model (Figure 2.3) defines three separate wake zones with differing expansion and decay rates to more accurately describe the velocity deficit across wind turbine rotors in wake regions. A major advantage of this model over Jensen's is its adaptability for handling of partial wakes and wake mixing which it achieves because of the three-zone

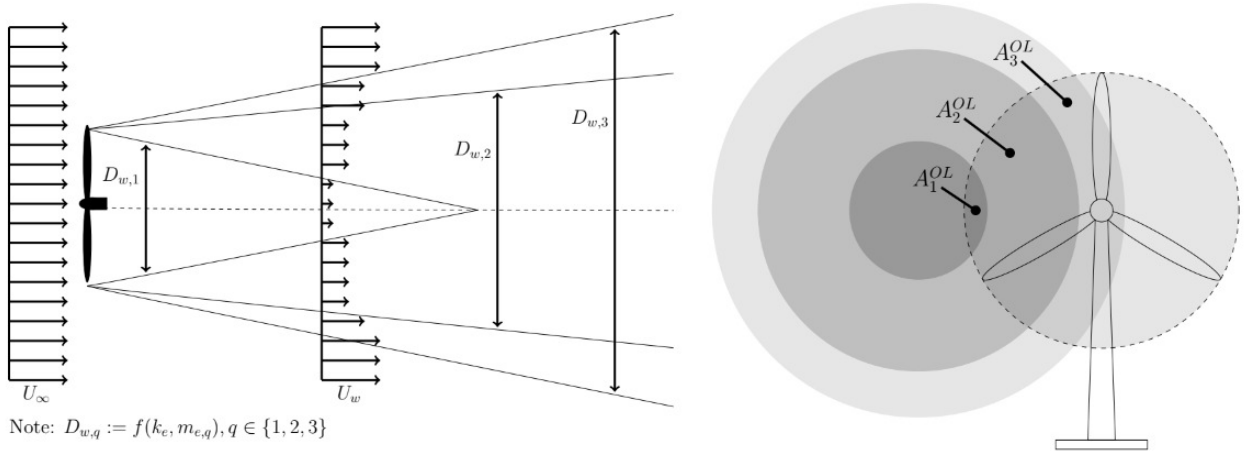

Figure 2.3: Schematic of the Floris wake model showing the three zones with varying diameters, $D_{w,q}$, and the overlap ratios, A_q^{OL} of each wake zone respectively.

Table 2.1: FLORIS wake model parameters

Parameter	value
$\mathbf{k_d}$, defines the sensitivity of the wake deflection to yaw	0.15
$\mathbf{a_d}$, wake at the rotor to be slightly offset from the rotor	-4.5
$\mathbf{b_d}$, rate of wake displacement if initial wake angle is not used	-0.01
$\mathbf{k_e}$, overall wake expansion	0.065
$\mathbf{m_{e,1}}$, $\mathbf{m_{e,2}}$, and $\mathbf{m_{e,3}}$, relative zone expansion	-0.5, 0.22, and 1
$\mathbf{M_{U,1}}$, $\mathbf{M_{U,2}}$, and $\mathbf{M_{U,1}}$, velocity deficit decay rates for each zone	0.5, 1, and 5.5
$\mathbf{a_U}$, zone decay adjustment parameter independent of yaw	5.0
$\mathbf{b_U}$, zone decay adjustment parameter dependent yaw	1.66

divisions. In this work, hub velocity losses due to waking were determined from the square root of the sum of squares of contributing losses which are determined using area weighted averages of the affected wake zones A_q^{OL}. The FLORIS wake model uses different parameters for characterizing wake deflection, expansion, and velocity. These parameters are found in Table 1 of [30], and presented here in Table 2.1. The FLORIS wake model agrees well with CFD simulation data when these parameters are used. Appendix B.1 shows a python execution of this wake model.

2.3 Flow Properties

Existing wind direction, speed, and frequency data was used to create a probability density function for wind direction, and a distribution for wind speed as a function of wind direction for

each of the three chosen locations (Figure 2.4). The locations are Victorville and Redding in California, and the setting of the Princess Amalia wind farm off the coast of the Netherlands.

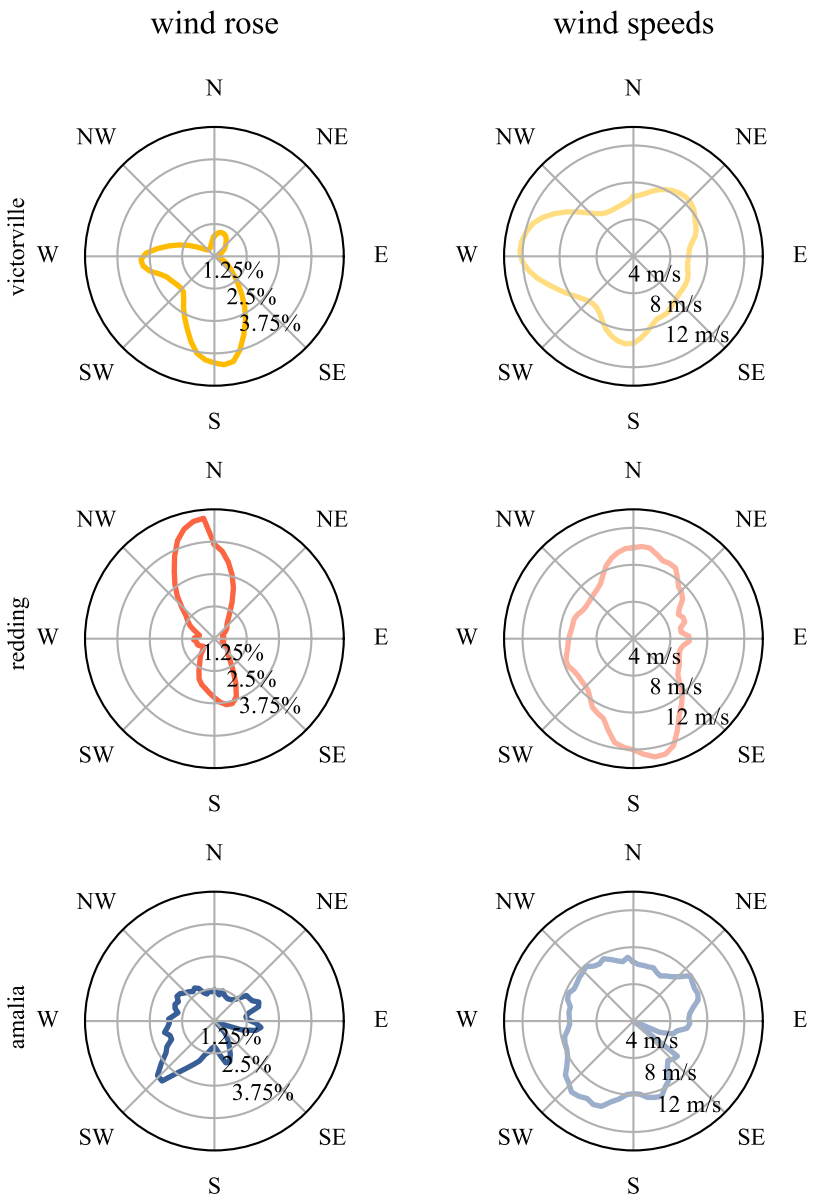

Figure 2.4: Denver, Redding, and Amalia, wind roses and directionally averaged wind speeds. The wind roses show the general source wind directions in relation to the frequency with which wind blows from a given direction. The directionally averaged wind speeds represent the magnitude of wind the speed coming from a given direction.

Since the power produced in a wind farm is largely dependent on wind conditions, the three wind roses chosen were dissimilar in order to measure the effectiveness of the variance reduction approach presented here under diverse conditions. The Amalia wind rose has multiple high probability directions with a wind speed profile closely matching the wind rose. Even though the Victorville and Redding wind roses each have two notably dominant wind directions, they are characterized by different orientations and wind speed profiles. These direction characteristics affect multi-modality in the design space in different ways.

The three different wind roses (Figure 2.4) were chosen to study optimization outcomes when this variance reduction concept is applied for different wind conditions. In order to maintain sampling consistency in each wind rose for numerical integration, data from each of these locations was splined using Akima splines [31] to obtain functional forms of wind frequency and speed, both of which depend on wind direction such that $f_{frequency} = f(direction)$, and $f_{speed} = f(direction)$. The resulting wind frequency function was then normalized to give the probability density function of wind frequency. A Python implementation of these formulations is given in Appendix B.2. In this work, 70 wind directions were selected between 0 and 360 degrees based on their probability and the corresponding directionally averaged wind speeds were determined from the wind speed function. These speeds represent the magnitude of the wind speed coming from a given direction as seen in Figure 2.4. Thus only wind direction uncertainty is considered in this analysis.

The resulting functions were normalized appropriately to give the probability density function of wind speed and frequency. In this work, 70 wind directions were selected between 0 and 360 degrees based on their frequencies, and their speeds were determined from the wind speed functions.

2.4 Statistics of Interest

Mean plant power is a major statistic of interest as it is used in determining quantities like annual energy production (AEP), net present value (NPV), cost of energy (COE), etc. It is a quantity that depends on the total farm power. The mean, although very useful, is only a measure of some central value and therefore does not paint a complete picture of the power producing capacity of a site. Together with the variance, the mean power can be interpreted to give more meaningful prediction of future power production since variance shows the spread from mean quantities. The

variance is thus a measure of risk in stochastic systems. The mean plant power is determined from the power contributions, P_i of all turbines in a farm.

$$P = \sum_{i=1}^{n_{turbs}} P_i. \tag{2.1}$$

$$P_i = \frac{1}{2}\rho A C_p U_i^3 \tag{2.2}$$

P_i is given by equation 2.2, where ρ is the air density and A is the rotor swept area. C_P, the power coefficient, is the power conversion efficiency of a wind turbine for which a value of 0.458 was used. The effective hub velocity for each turbine is U_i. It is a function of position (x and y) as well as flow parameters and variables (wind direction and speed β and U_∞ respectively). The values of U are determined with the FLORIS wake model mentioned above. Appendix B.3 shows the power calculation in Python. Because of the probabilistic nature of wind direction, the mean plant power can be expressed as an integral for a random variable (equation 2.3).

$$\mu_P = E[P] = \int_0^{2\pi} P(x,y,\beta,U_\infty)\ \phi(\beta)\ d\beta \approx \sum_{j=0}^{m} P(x,y,\beta_j,U_{\infty,j})\ \phi(\beta_j) \tag{2.3}$$

In this equation, $\phi(\beta)$ is the probability density function of the wind direction and m is the number of sampled wind directions. Again because of the stochastic nature of wind direction, the mean power can be accurately calculated using different integration schemes and other uncertainty quantification techniques including, Monte Carlo integration (MC), polynomial chaos expansions, and the rectangle rule for numerical integration. Each of these methods have their pros and cons. MC is simple but often inaccurate unless large sample sizes ($10,000s$ to $100,000s$ depending on the size and complexity of the problem) are used, in which case computational cost increases. The rectangle rule however is generally more accurate at lower sample sizes ($10s$ to $100s$), and is relatively computationally inexpensive. PC is in the middle ground because of lower computational cost and sample size for accuracy. The mean power is simply expressed as an integral for determining the mean of a random variable since the density function of wind direction is known. This integral can be evaluated as that for a discrete random variable using the rectangle rule (far right hand side of equation 2.3) since samples are drawn from the wind distributions in this analysis.

Each wind direction β_j has a corresponding directionally averaged free stream wind speed $U_{\infty,j}$ which is determined form the wind speed distribution. The uncertain variable of interest here is the wind direction β, making this a 1-dimensional uncertainty quantification problem.

The variance is evaluated similarly from the integral given in equation (2.4). A Python implementation of these equations is given in Appendix B.4

$$\sigma_P^2 = \int_0^{2\pi} P^2(x,y,\beta,U_\infty)\ \phi(\beta)\ d\beta - \mu_P^2 \approx \left(\sum_{j=0}^{m} (P^2(x,y,\beta_j,U_{\infty,j})\phi(\beta_j) \right) - \mu_P^2 \qquad (2.4)$$

2.5 Optimization Framework

Multi-objective optimization (MOO) problems are those that involve more than one objective function to be minimized. In optimization, minimizing is the general expression used since minimizing the negative of a function corresponds to maximizing it. MOO problems are typically expressed mathematically as

$$\begin{aligned} &\min\ (f_1(x), f_2(x), ..., f_k(x)), \qquad k \geq 2 \\ &\text{s.t. } x \in \mathbf{X} \end{aligned} \qquad (2.5)$$

where k is the number of objective functions and $\mathbf{X}$ is the set of feasible decision vectors and/or constraint set. Such problems have multiple solutions that quantify the best tradeoff between competing objectives as opposed to global optima found in single-objective optimization problems. Because of the existence of a set of solutions, the concept of dominance is introduced to determine if one solution is better than another. For two solutions x_1 and x_2, x_1 is said to dominate x_2 if x_1 is better than x_2 in at all objectives.

Another useful concept in MOO is "Pareto optimality". This defines the quality of solutions in the feasible objective space based on their dominance. The following definitions (presented in [32]) are given for Pareto optimality.

- **Definition 1** Pareto Optimal: A point, $x^* \in \mathbf{X}$, is Pareto optimal if and only if no other point $x \in \mathbf{X}$ exists, such that $\mathbf{f}(x) \leq \mathbf{f}(x^*)$, and $f_k(x) \leq f_k(x^*)$ for at least one of the opposing functions [33].

- **Definition 2** Weakly Pareto Optimal: A point, $x^* \in \mathbf{X}$, is weakly Pareto optimal if and only if no other point $x \in \mathbf{X}$ exists, such that $\mathbf{f}(x) \leq \mathbf{f}(x^*)$ [33].

Pareto optimal solutions are therefore sets of solutions that cannot be dominated by any others in the design space. This set of solutions is referred to as a Pareto front (Figure 2.5). Depending on the design space and the choice of optimization algorithm, solutions MOO problems may satisfy some design criteria but may not necessarily be Pareto optimal in the sense of Definition 1 [32]. For example, there may be points in the objective space that improve some objectives but do no change others [33]. Such solutions are referred to as weakly Pareto optimal solutions in contrast to Pareto optimal solutions where no other point in the design space can improve at least one objective function without penalizing another. Thus, the set of Pareto optimal solutions is the super set of which weakly Pareto optimal solutions form a subset. The following resources give in-depth details about MOO and Pareto optimality [32, 33]

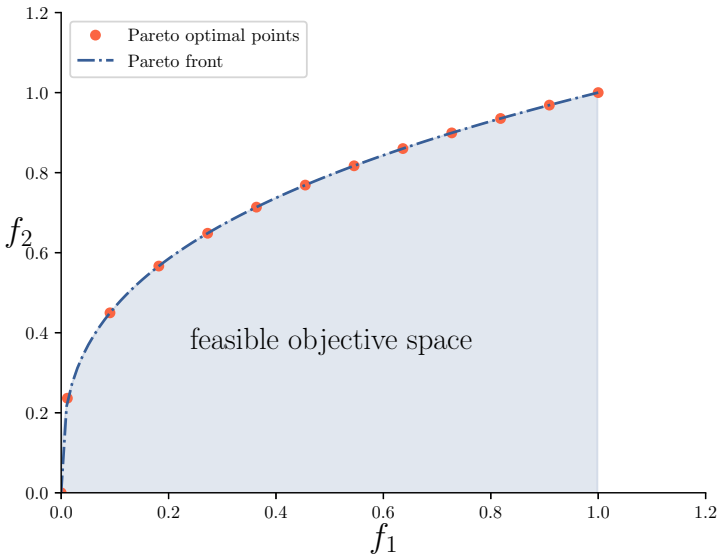

Figure 2.5: Pareto front of two opposing objectives in the feasible objective space. The functions f_1 and f_2 are being minimized and maximized respectively.

Some standard approaches to solving MOO problems include: normalized objective functions, the weighted sum method, $\varepsilon-$constraint method, lexicographic method, multi-objective evolutionary algorithms, and the normal boundary intersection method. Further details about the

strengths and weaknesses of these methods can be found in [32, 34]. In this work, however, the $\varepsilon-$constraint method is used due to its simplicity, and effectiveness in both convex and non-convex design spaces.

2.5.1 ε-constraint Method for Pareto Optimization

The $\varepsilon-$constraint method of MOO (equation 2.6) involves minimizing just one objective with inequality constraints which are formulated from the other objective functions. In this work the main objective to be minimized is the variance, thus ε values are chosen for mean plant power. However, the ε values are themselves obtained from prior mean plant power optimizations.

$$\begin{aligned} &\text{minimize} && f_2(\mathbf{x}), \\ &\text{subject to} && f_1(\mathbf{x}) \leq \varepsilon_i \\ &\text{w.r.t} && x_j, \qquad j = 0, 1, 2, ..., n \end{aligned} \tag{2.6}$$

Using this method, three optimization steps were used to obtain sets of weakly Pareto optimal solutions in this work. The first optimization involves maximizing the mean power only without any constraints on the variance, and the second is minimizing the variance with no constraint on the mean power. In each case, 100 starting layouts were used to determine the maximum and minimum values respectively. These two initial optimizations provide the anchor points[2] for a Pareto front. For this problem, both $\mu_{P,\ step\ 1}$ and $\sigma^2_{P,\ step\ 1}$ are greater than $\mu_{P,\ step\ 2}$ and $\sigma^2_{P,\ step\ 2}$. Step 3 is the final one where the variance is minimized with inequality constraints set on the mean power. The mean power inequality constraint is from the first mean power optimization. These steps are presented in equations 2.7, 2.8, and 2.9.

[2]These are the two extreme points on the curve, one corresponding to the lowest mean power and variance, and the other, to the highest mean and associated power variance.

- **step 1**: maximize the mean farm power with no constraint on variance

$$\begin{aligned} &\text{maximize} && \mu_P^* \\ &\text{w.r.t} && x_i, y_j \quad i,j = 0,1,2,...,n_{turbs} \\ &\text{subject to} && S_{i,j} \geq 2D_{turbine}, \quad i,j = 0,1,2,...,n_{turbs} \\ & && boundary\ \ constraints \end{aligned} \tag{2.7}$$

- **step 2**: minimize variance with no constraint on mean power

$$\begin{aligned} &\text{minimize} && \sigma_P^2 \\ &\text{w.r.t} && x_i, y_j \quad i,j = 0,1,2,...,n_{turbs} \\ &\text{subject to} && S_{i,j} \geq 2D_{turbine}, \quad i,j = 0,1,2,...,n_{turbs} \\ & && boundary\ \ constraints \end{aligned} \tag{2.8}$$

- **step 3**: minimize variance with constraint on mean power starting with the solution from step 1

$$\begin{aligned} &\text{minimize} && \sigma_P^2 \\ &\text{w.r.t} && x_i, y_j \quad i,j = 0,1,2,...,n_{turbs} \\ &\text{subject to} && \mu_P \geq \mu_{P_{reduced}} \\ & && S_{i,j} \geq 2D_{turbine}, \quad i,j = 0,1,2,...,n_{turbs} \\ & && boundary\ \ constraints \end{aligned} \tag{2.9}$$

Where $S_{i,j}$ is the distance between each pair of turbines i and j set to no less than 2 rotor diameters for the n turbines in the wind farm. The ε values, $\mu_{P_{reduced}}$ were determined by reducing μ_P^*, to obtain evenly spaced values between $\mu_{P,\ step\ 1}$ and $\mu_{P,\ step\ 2}$. Step 3 was repeated for each of the ε values to produce the Pareto fronts. The placement of each turbine is also constrained to positions only within the farm boundaries which are either circular or square in each case.

2.5.2 Variance Reduction Concept

The approach presented below is a simple yet very rewarding variance reduction technique for power forecasting through wind farm layout optimization. The method is a form of the ε-constraint method of multi-objective optimization given above, where an initial optimization is used to determine the epsilon values. In this approach, however, an entire Pareto front is not developed. There is also no reduction in mean power during the variance minimization step. Thus the $\varepsilon-$constraint method is effectively applied by taking advantage of multimodality to force the optimization to reproduce a solution with the output of the previous mean power but with a lower variance.

In this work, the main objective to be minimized is the variance. The optimization is carried out in two steps. Step 1 is the common practice of maximizing mean plant power without any constraints set on the variance. This first optimization gives a suitably high mean power value with a corresponding variance that is usually high. Step 2 then aims at reducing the variance associated with the mean power from step 1. This is done by performing a second optimization where the variance is minimized with an inequality constraint set on the mean power to be greater than or equal to the value from step 1. Also, the starting layout in this second optimization is the solution from the step 1 problem. The combined optimization problem is formulated below as:

step 1: Maximizing mean power

$$\begin{aligned} &\text{maximize} && \mu_P^* \\ &\text{w.r.t} && x_i, y_j \quad i,j = 0,1,2,...,n_{turbs} \\ &\text{subject to} && S_{i,j} \geq 2D_{turbine}, \quad i,j = 0,1,2,...,n_{turbs} \\ & && boundary\ \ constraints \end{aligned} \tag{2.10}$$

step 2: Variance reduction

$$
\begin{aligned}
&\text{minimize} && \sigma_P^2 \\
&\text{w.r.t} && x_i, y_j \quad i,j = 0,1,2,...,n_{turbs} \\
&\text{subject to} && \mu_P \geq \mu_P^* \\
& && S_{i,j} \geq 2D_{turbine}, \quad i,j = 0,1,2,...,n_{turbs} \\
& && boundary\ \ constraints
\end{aligned}
\tag{2.11}
$$

By doing this, we are able to obtain better solutions, i.e., layouts that produce effectively the same high wind power but with lower variance than in the case of performing a single mean power optimization. The degree of improvement seen after the variance reduction step varies with each case. Naturally, some combinations of wind combination, farm boundary, and size show greater improvement over others.

The Python Optmization Sparse framework (pyOptSparse) [35] was used with Sparse Nonlinear Optimizer (SNOPT), a gradient-based fortran software package for solving large-scale nonlinear optimization problems [36], to perform all the optimizations in this work.

CHAPTER 3. RESULTS AND DISCUSSION

This section shows results for variance reduction in wind farm layout optimization using the proposed variance minimization concept. Simulations were carried out for different combinations of farm sizes, boundaries, and wind roses. Also presented are results for variance reduction using a full Pareto optimization.

3.0.1 Variance Reduction

As discussed, wind farm layout optimization typically seeks to optimize a metric related to the mean or expected power, like the annual energy production or cost of energy. However, because the design space is multimodal it is good practice to use a multistart procedure, where many random starting points are used and the best result is then taken. In this work 100 random starting points were used in each case to first optimize wind farm layouts for maximum mean power. Those multiple starting locations created a range of values as shown in Figure 3.1 for a 36-turbine wind farm with Amalia wind conditions in a circular boundary. The key insight of this work is that those same solutions, which maximize mean power have very different variance. This can be seen in Figure 3.1 where the percentage difference between the normalized[1] maximum and minimum mean power is about 2.5%, and that between the variance maximum and minimum is about 10%.

We can exploit this behavior even further by minimizing the variance while constraining the mean power. In Figure 3.2 we see that the mean power remains the same, whiles the variance changes after performing a second optimization with constraints set on the mean. The variance values from the μ_P maximization step are noticeably larger than those from the variance reduction step. This is more apparent in the right window where gray arrows show the shift in variance between the first and second optimizations for 10 instances.

[1] Both mean power and variance are normalized by the highest mean power and variance respectively from the step 1 optimizations

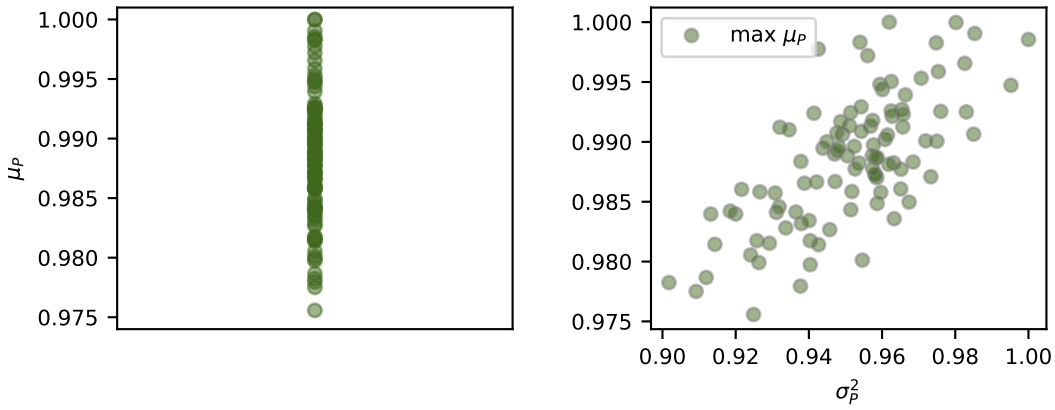

Figure 3.1: (left) Normalized mean power results from 100 layout optimizations for a 36−turbine, circular boundary farm using the Amalia wind conditions. (right) Mean power and corresponding variance from the same 100 optimizations (each normalized by the highest mean and variance respectively from the step 1 optimizations, where only the mean power was maximized with no constraints on the variance). The difference between maximum and minimum variance values is noticeably larger than that between mean power values.

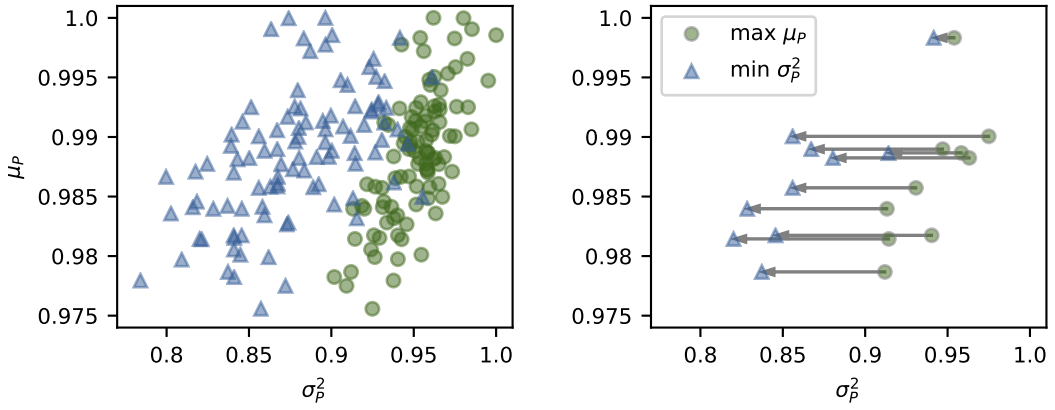

Figure 3.2: Normalized mean power and variance from the two optimization steps of maximizing mean power, and reducing variance. The second optimization variance results are generally lower than those from the first while the mean power stays the same in both optimizations. The right window shows this shift clearly for 10 pairs of optimizations.

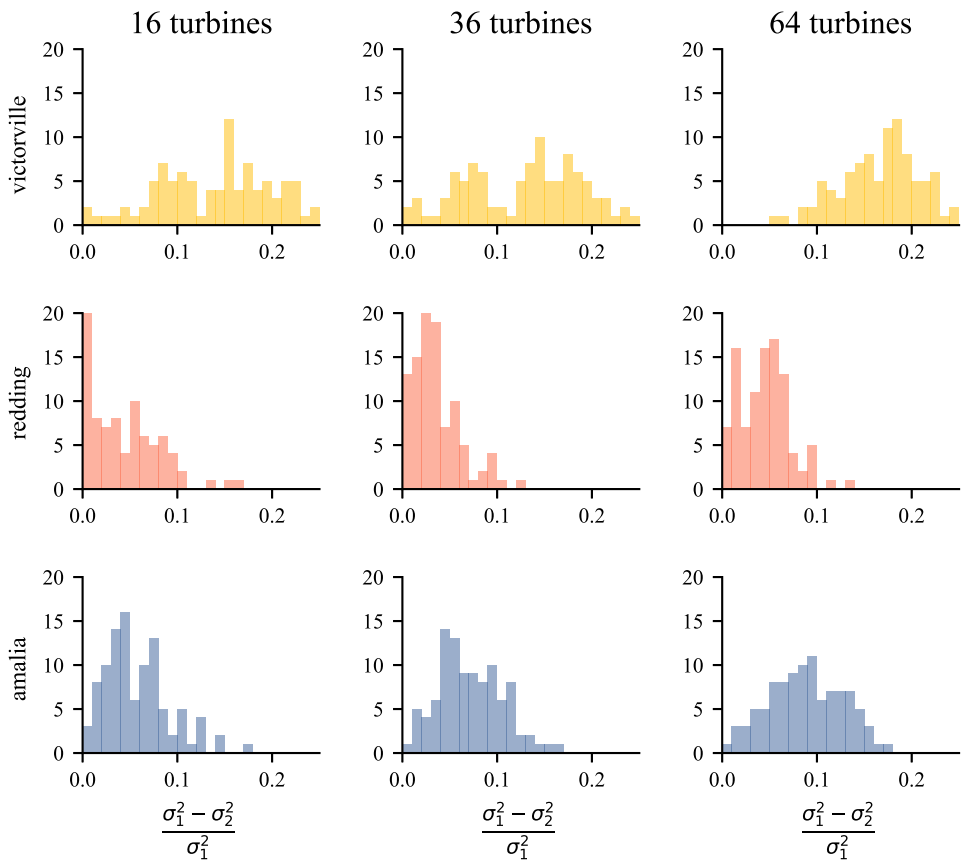

Figure 3.3: Relative variance decrease for circle farm boundary cases.

This trend of lowered variance after performing two sequential optimizations is observed in all the cases considered. Table 3.1 contains the minimum, average, and maximum relative[2] reduction in variance for 18 cases which consist of 16-, 36-, and 64-turbines in both circle and square farm boundaries with the wind conditions from the three locations (Victorville, Redding, and Amalia wind farm). The land area of each wind farm is based on the area of a square grid arrangement of wind turbines with an approximate initial spacing of 5 rotor diameter spans. Thus both circle and square boundaries with the same number of turbines have the same area.

There is nonzero variance decrease in all the cases analyzed although some reductions are smaller than others. Also, a wider range of variance reduction is observed in some cases over others. In Figure 3.3, we observe that the Victorville and Amalia wind roses yield wider ranges of relative variance decrease compared to the bidirectional Redding cases. The Victorville farms

[2]Reduction in variance is measured relative to the power variance from maximum mean power optimization.

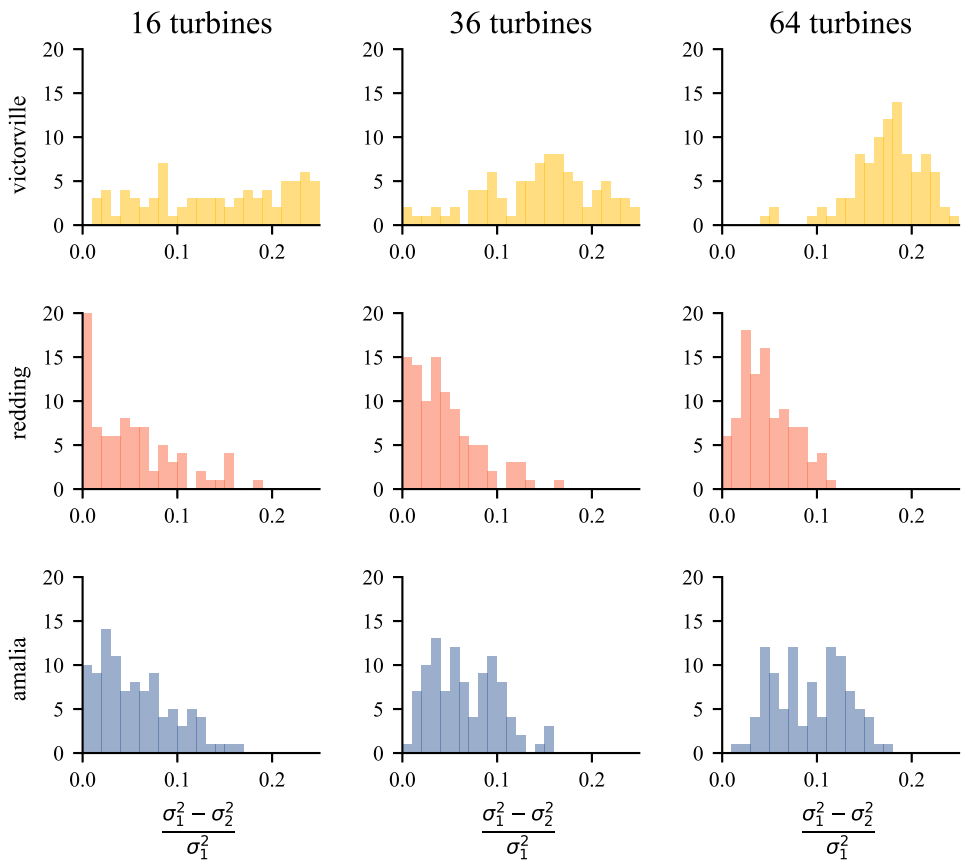

Figure 3.4: Relative variance decrease for square farm boundary cases.

generally produce the highest variance decreases of up to 20%. The Redding cases produce lower variance reductions in comparison to the other two wind roses. This is because multidirecional wind roses further increase the occurrence of local minima in the design space. Thus, allowing for more distinct solutions that yield high mean power at different variances.

The square cases (Figure 3.4) show similar trends as the circle ones with the Victorville and Amalia farms again favoring variance reduction over the Redding farms.

The wind farm layout optimization process creates a pattern for arranging turbines within a boundary that promotes high power output. Figure 3.5 shows optimized layouts for 36-turbine circle and square farm boundaries respectively. The mean power stays the same for the two optimization steps as previously mentioned, whereas the variances[3] after the second optimization are

[3]Presented here as the standard deviation for consistency of units.

Table 3.1: Minimum, average, and maximum % change in plant power variance for 16−, 36−, and 64-turbine circle and square boundary wind farms and all three wind roses from 100 individual layout optimizations using the proposed two step variance reduction approach.

boundary	wind rose		16	36	64
		min	0.520	0.230	5.53
	Victorville	avg	14.6	12.7	17.2
		max	29.9	24.8	27.9
			0.00340	0.0244	0.377
circle	Redding		3.82	3.49	4.56
			16.7	12.2	13.6
			0.517	0.949	0.434
	Amalia		5.74	7.14	8.81
			17.4	16.1	17.6
		min	1.23	0.508	4.54
	Victorville	avg	16.8	15.0	17.8
		max	33.3	30.3	27.6
			0.00660	0.0270	0.141
square	Redding		4.31	4.46	4.69
			18.2	16.1	11.1
			0.00830	0.533	1.46
	Amalia		5.61	6.63	9.30
			16.2	15.8	17.6

noticeably less than those in first. Each layout solution is indicative of the shape of the wind rose used.

In the Victorville and Amalia wind roses, we observe that turbines are more evenly spread within the farm boundaries. This is a consequence of their wind direction and wind speed profiles. The diagonally symmetric bidirectional Redding wind rose has turbines at the boundary edges, and in the middle of the farm as expected. Turbines are arranged within farm boundaries such that rotor-on-rotor wake interactions are minimized in order to promote energy capture.

Lastly, the square farms generally yield higher mean power than their circle counterparts for each of the wind conditions even though the land areas are equal. This is because the angled corners

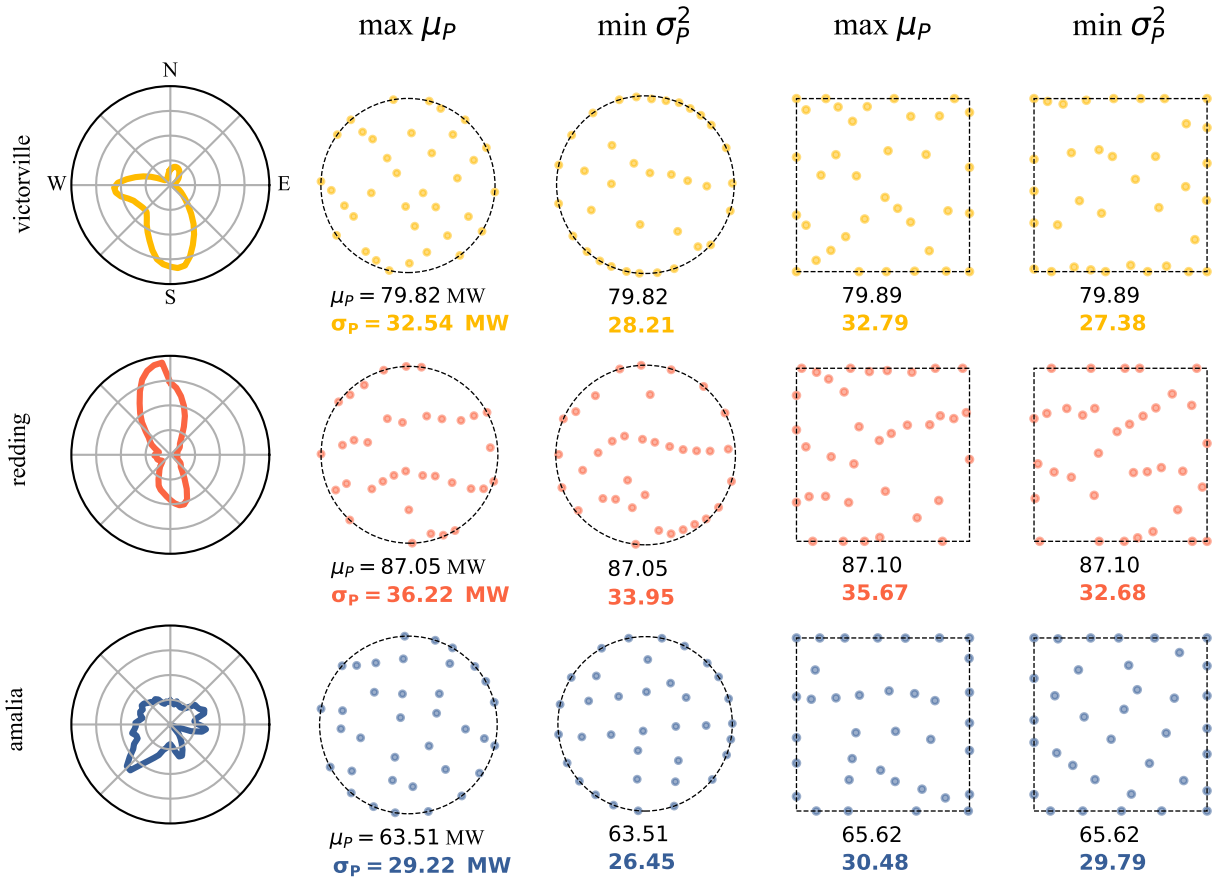

Figure 3.5: Layout optimization solutions for 36-turbine circle and square farms using the Victorville, Redding, and Amalia wind conditions. Step 1 and 2 solutions are shown with their corresponding mean power and standard deviation.

in the square boundaries offer better turbine separation, which in turn reduces the occurrence of wakes.

This is the main advantage of applying this concept to the wind farm layout optimization problem–there is no reduction in mean power for a corresponding decrease in variance. The approach yields positive results because the wind farm layout optimization design space is highly multi-modal. Hence, although multi-modality makes optimization problems more difficult, it can be exploited to minimize variance in long-term wind power forecasting.

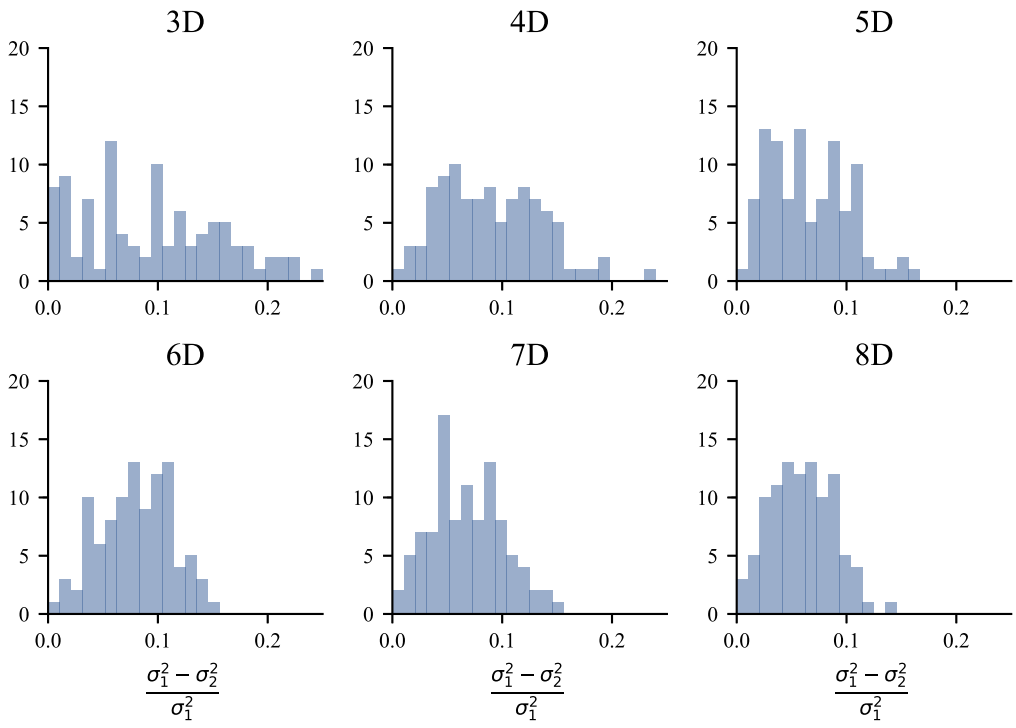

Figure 3.6: Relative variance decrease for different turbine densities based on 3–8 rotor diameter spacings for circle Amalia farms.

3.0.2 Variance Reduction with Different Turbine Densities

A few cases were also studied using the proposed concept with different turbine densities, meaning the same number of turbines are confined to different land areas. The presented optimization results are for the Amalia wind rose, and 36-turbine farms. Wind farms with six different turbine densities were studied, with average turbine spacings of 3–8 rotor diameters (Figure 2.2).

The relative differences in variance between the two optimization steps for the different turbine densities for a circle boundary farm are presented in Figure 3.6. The denser (5D spacing and below) farms yield a wider range of relative variance decrease over the sparser ones (6D spacing and above). These denser farms also show higher average variance decreases, with the largest being approximately 9% for the farms with 3-rotor diameter average spacing. The lowest average variance decrease is just over 5% as seen in the farms with 8-rotor diameter average spacing.

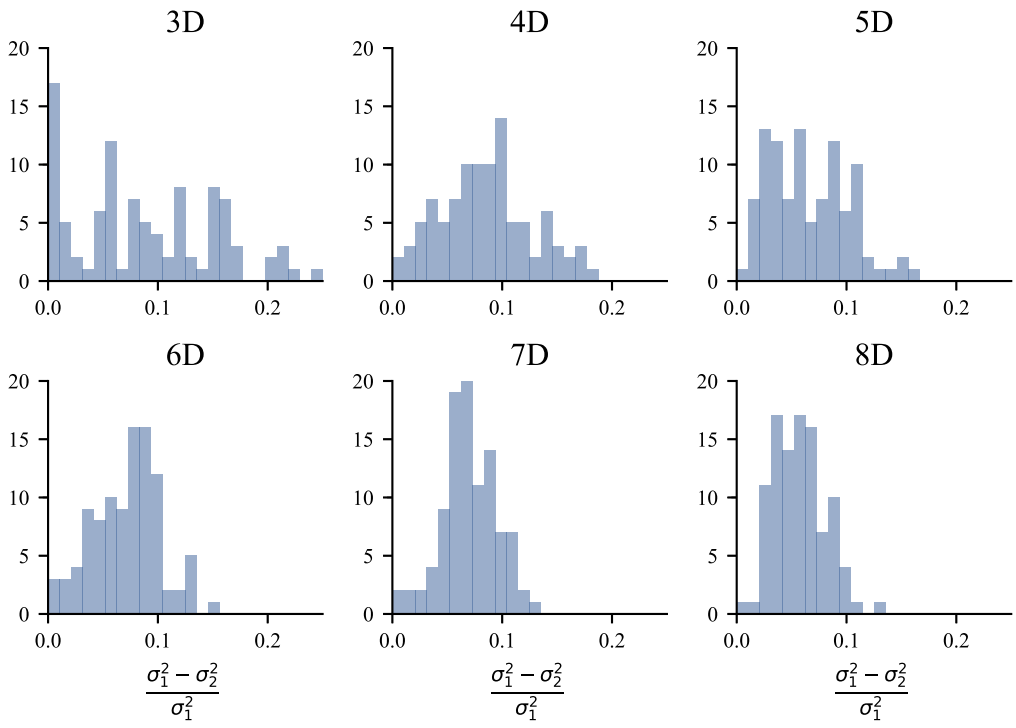

Figure 3.7: Relative variance decrease for different turbine densities based on 3–8 rotor diameter spacings for square Amalia farms.

Figure 3.7 shows the variance reduction results for varied turbine spacing in square wind farms. As with the circular farms, the average variance reduction is inversely proportional to turbine density. However, even for the farms with larger average turbine spacing, a large variance reduction was achieved.

The denser wind farms achieve larger variance reduction than the sparser farms. This is because of the strong wake effects that exist in denser wind farms. When the turbines are close together, the turbine wakes have not had a chance to recover before reaching downstream turbines. Thus, as the wind changes direction the power production changes more drastically, as turbines move in and out of the strong wakes of upstream turbines. In wind farms where the turbines are spaced farther apart, wakes have more time to recover before interacting with downstream turbines. This means that the power production is not affected as much by turbine wakes.

3.0.3 Comparison to Pareto Optimization

The previous sections demonstrated that after optimizing a wind farm layout for maximum power production, the variance can be significantly reduced by re-optimizing the layout for minimum variance. By constraining the mean power, this variance reduction can be achieved without any sacrifice to mean performance. This process is very simple, and can be done using existing wind farm models and optimization frameworks for very little additional effort. However, if one has the computational resources and is willing, further insight can be gained by performing a full multi-objective optimization and finding the Pareto front of the design space.

Pareto optimal results offer the best possible compromise between two objectives. A Pareto front is computationally expensive to generate, requiring thousands of individual optimizations. The black points in Figure 3.8 represent the approximate Pareto front for a 36-turbine wind farm with square boundaries, five rotor diameter average turbine spacing, and using the Amalia wind data. These data are close to the lowest variance solution that can be found with certain constraints on the mean power. They were generated by constraining the mean wind farm power to different values, and minimizing the associated power variance.

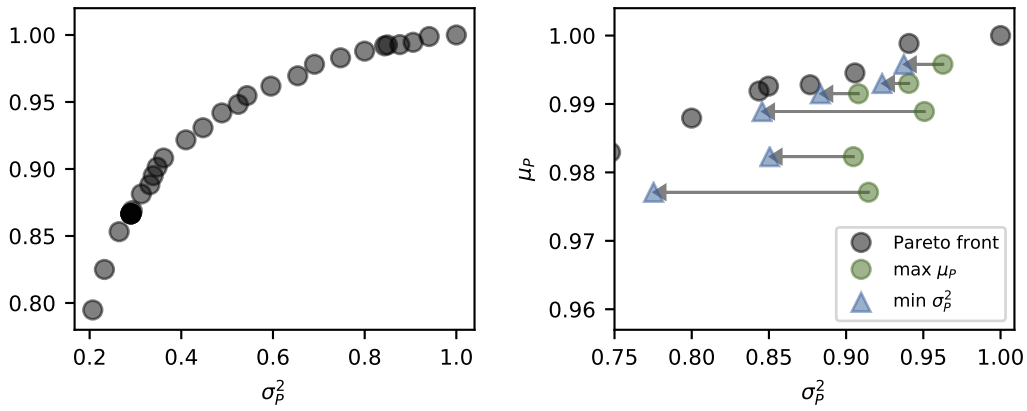

Figure 3.8: Pareto front for the multi-objective wind farm layout optimization problem of high mean power versus low variance on 36-turbine square boundary farm using the Amalia wind conditions. Also shown are six pairs of points from mean power and variance optimizations.

As can be seen, a point on the Pareto front cannot achieve lower variance for the same mean power. The objectives of maximum mean and minimum variance conflict, meaning that

to improve one objective you must sacrifice some of the other. For this wind farm, and the others considered during this study, the Pareto front is relatively flat near the upper right hand corner. This is significant, as it means that if one is willing to sacrifice a small amount of mean power production they are able to greatly reduce the variance. For the case shown in Figure 3.8, a 2% sacrifice in the mean power can result in more than 25% decrease in variance. Much larger reductions in variance can be achieved, but they come at a higher cost in mean power.

For wind farms, the region of the Pareto front of most interest is the upper right corner, the solutions with high mean power. The right sub-figure in Figure 3.8 shows a zoomed in portion of this upper right corner. When performing an optimization to maximize the mean power of the wind farm (step 1 of the method presented in this paper), the solution is somewhere near this portion of the Pareto front. A few of these solutions are shown in Figure 3.8 with the green dots. When step 2 of our method is applied, a new solution is found with lower variance. The solution from step 1 is pushed closer to the Pareto optimal. Because this upper portion of the Pareto front is relatively flat, this method can produce large variance reduction, even for the higher mean power solutions.

In the context of full multi-objective optimization, the method presented in this work is extremely useful. Rather than seek to fully explore the design space, and trade-offs that exist between the mean and variance, one can simply apply this method. This will produce a wind farm layout with high mean power, as well as variance that approaches the Pareto optimal solution, with greatly reduced computational expense.

CHAPTER 4. CONCLUSION

This work explored a simple, yet efficient approach to reducing variance in wind farm layout optimization. The different cases that were evaluated demonstrate the effectiveness of this approach for different farm boundaries, turbine counts, and wind conditions. Although there are standard variance reduction techniques such as antithetic and control variates, and common random numbers [22], the problem was treated as a multi-objective optimization problem for two objective, namely, maximizing mean power and minimizing/reducing variance. This approach led to solutions with lower variance and at no expense to the mean-plant-power in a simpler and faster fashion.

The mean-plant-power is a major statistic of interest during the design and development stages of wind farm as it is used in determining quantities of interest such as AEP, COE, NPV, etc. In general high values of mean power are sought in layout optimization for power forecasting purposes. Turbine placement, i.e., wind from layout optimization, is a significant step in wind farm design since intelligently situating turbines can improve the energy capture capacity of a site. Because mean power does not provide information about the potential power fluctuations in a wind farm, it is instructive to study the associated variance (standard deviation) to get a sense of the risk associated with this quantity in power forecasting. A low variance will translate to better stability of forecasts and thus variance should be lowered where possible.

This thesis examined the effects of farm size, wind conditions, and farm boundary type on variance minimization for mean-plant-power forecasting during wind farm layout optimization. The two-step approach presented above uses constraints on the mean power to minimize the variance during wind farm layout optimization. It involves two optimizations where the first is a layout optimization for maximizing mean-plant-power. The second step is to re-optimize the wind farm layout to minimize power variance. In this step the mean power is constrained to be greater than or equal to the mean power achieved in the first step. This means that a wind farm layout with both

high mean power and low variance can be found. The success of this two-step process is enabled by the multi-modality of the wind farm layout design space. Because the wind farm layout optimization design space is highly multi-modal, many solutions can be found that yield comparable power outputs but very different power variances. The method presented in this thesis finds the less volatile solutions, i.e., solutions that correspond to the lower power variances.

The proposed framework was tested on different wind farm sizes (i.e., farm boundary types and turbine counts) with three different wind conditions. Results for all the different cases studied show that this method is effective at reducing the variance while maintaining the initial high mean power. In every case that we considered, there was a noticeable average decrease in wind-plant-power variance between step one and step two of our method. It was also observed from this analysis that variance reduction in wind farm layout optimization improves for regions where the wind conditions are characterized by high variability. This was seen in the results from the Victorville and Amalia cases that showed higher average variance reduction. For the 64-turbine wind farms, the Vitorville wind farms achieved over 17% average variance reduction, and the Amalia wind farms over 8% average variance reduction. The Redding wind farms experienced a lower average variance reduction, of about 4.5% for both circle and square farm boundaries.

For the cases with different turbine densities, there was an overall decrease in variance after performing the two sequential optimizations. The denser wind farms experienced greater power variance reductions between steps one and two of the method. For both wind farm boundaries, the average variance decrease in the 3D farm was highest, about 9%. The wind farms with turbines spaced farther apart still noticeably reduced the variance between the two steps, although by a smaller percentage. The largest turbine spacing of 8 rotor diameters achieved an average variance reduction of about 5%. This indicates that this method will therefore be more beneficial to situations where land is scarce and turbines would need to be built close together. However, even wind farms with turbines spaced far apart can benefit greatly from the presented methodology.

It was also shown that the problem can be solved using Pareto optimization–a standard method for tackling multi-objective optimization problems. The Pareto approach presents a pictorial view of the solutions from opposing objectives to clearly define the trade-offs between them as there is no single "best" solution. There is rather a set of solutions that shows the best compromise between objectives; in this case mean-plant-power and variance. This set of results offers the best

compromise between opposing objectives. From the Pareto optimization example we can see that improved wind farm layouts can be obtained that produce relatively lower power at much lower variances. The greater the sacrifice in mean power, the higher the reduction in the associated variance. This reduction in power production is, however, left to the discretion of policy makers. Thus a developer can decide how much sacrifice they are willing to make in order to obtain more reliable long-term power forecasts. But the results show that the results we typically obtain from individual mean-plant-power maximizing optimizations are closer to the high power Pareto solutions, i.e., the top 2% mean power values. Thus developing an entire Pareto front may not be necessary in many cases. Instead, applying the proposed method gives solutions that are sufficiently close to the Pareto optimal ones.

It is clear from this analysis that reduction of power variance in wind farm layout optimization improves for wind conditions with more variability. This is observed in the results from the Victorville and Amalia cases that showed higher average variance reduction in general. Secondly, there is some reduction observed in all cases although some combinations of farm sizes, boundaries, and wind conditions tend to favor reduction with this approach more than others.

This concept is meant to be used to improve the accuracy of long-term power forecasting through wind farm layout optimization. The method is an extremely simple and easily implementable one that significantly reduces wind farm power variance. Beacuse some simplifying assumptions were made to demonstrate the intended concepts, the following recommendations are suggested for more indepth future works.

- **Applying this process to operational wind farms.** Although the choice of turbine and wake model in this work closely match those used in practice, real wind farms are somewhat different in their boundaries and flow conditions.With the exception of the Amalia wind data, the other two data sets are not representative of the climate and weather conditions of real wind farm sites. It would therefore be instructive to test this framework on real farms to serve as a further step in validating the concept presented here.

- **Considering uncertainty in both wind speed and wind direction in applying this process.** Although this will be a complicated uncertainty quantification problem, it will present

a more realistic case as the wind resource is characterized by more than the one form of uncertainty covered here.

- **Exploring different numerical integration methods with the aim of improving computation speed and accuracy during optimization.** The integrals for mean-plant-power and variance are evaluated several times during an optimization. They also become more complicated when uncertainty in higher dimensions is considered. Therefore, finding a good integration scheme that offers the best compromise between computation speed and accuracy would enhance some of the inner workings of this process.

APPENDIX A. WIND FARM LAYOUT OPTIMIZATION OBJECTIVE FUNCTIONS

1. Total farm power, P

$$P = \sum_{i=1}^{n_{turbs}} P_i \tag{A.1}$$

$$P_i = \frac{1}{2}\rho \times A \times C_p \times U_i^3 \tag{A.2}$$

- ρ = the air density
- A = rotor swept area
- C_P = power coefficient

2. Expected power, $E[P]$

$$\mu_P = E[P] = \int_0^{2\pi} P(x,y,\beta,U_\infty)\ \phi(\beta)\ d\beta \approx \sum_{j=0}^{m} P(x,y,\beta_j,U_{\infty,j})\ \phi(\beta_j) \tag{A.3}$$

3. Annual energy production (AEP)

$$AEP = 8760\frac{hr}{yr} \times E[P] \tag{A.4}$$

4. Net present value (NPV)

$$NPV = -K + \sum_{k=1}^{L} \frac{(H \times E[P] \times P) - M}{(1+r)^{k-1}} = -K \sum_{k=1}^{L} \frac{F}{(1+r)^{k-1}} \tag{A.5}$$

$$F = (H \times T \times P) - M \tag{A.6}$$

- H = total operating time period (8760 hr/yr)
- K = total investment in wind farm (land and turbine cost, installation costs, etc.)

- L = lifetime of turbines
- M = cost of operation and maintenance
- P = the unit sale price of electricity
- r = financial interest rate

5. Profit

$$Profit = AEP \times k - \frac{Cost_{TOT}}{T} - M \tag{A.7}$$

- k = estimated selling price for 1 MWh of electricity
- $\text{Cost}_{TOT} = \text{Cost}_{1MW} \times \text{MW}_{installed}$
- T = lifetime time in years
- M = operations and maintenance costs

6. Levelized cost of energy (LCOE)

$$LCOE = \frac{\frac{I_t + M_t + F_t}{(1+r)^t}}{\sum_{t=1}^{n} \frac{E[P]_t}{(1+r)^t}} \tag{A.8}$$

- I_t = investment expenditures in year, t
- M_t = operations and maintenance costs in the year
- F_t = Fuel expenditure in the year, t
- $E[P_t]$ = expected electricity generation in the year, t
- r = discount rate
- n = economic life cycle of the system

APPENDIX B. PYTHON IMPLEMENTATIONS OF KEY ALGORITHMS

The following are Python implementations of the main algorithms used in this work.

B.1 FLORIS wake model call

```
1
2  def Floris(turbineXw, turbineYw, turbineZ, rotorDiameter, Vinf, yaw=False,
       Ct=False, kd=0.15, bd=-0.01, initialWakeDisplacement=-4.5,\
3              useWakeAngle=False, initialWakeAngle=1.5, ke=0.065,
     adjustInitialWakeDiamToYaw=False, MU=np.array([0.5, 1.0, 5.5]),\
4              useaUbU=True, aU=5.0, bU=1.66, me=np.array([-0.5, 0.22, 1.0]),
       cos_spread=1.e+12, Region2CT=0.888888888889, axialInduction=False, \
5              keCorrCT=0.0, keCorrArray=0.0, axialIndProvided=True,
     shearCoefficientAlpha=0.10805, shearZh=90.):
6      """floris wake model"""
7      nTurbines = len(turbineXw)
8
9      if yaw == False:
10         yaw = np.zeros(nTurbines)
11     if axialInduction == False:
12         axialInduction = np.ones(nTurbines)*1./3.
13     if Ct == False:
14         Ct = np.ones(nTurbines)*4.0*1./3.*(1.0-1./3.)
15
16     # yaw wrt wind dir.
17     yawDeg = yaw
18
19     nSamples = 1
20     wsPositionXYZw = np.zeros([3, nSamples])
21
```

```
    # call to fortran code to obtain output values
    wtVelocity, wsArray, wakeCentersYT, wakeCentersZT, wakeDiametersT, wakeOverlapTRel = \
                _floris.floris(turbineXw, turbineYw, turbineZ, yawDeg, rotorDiameter, Vinf,
                                                    Ct, axialInduction, ke, kd, me, initialWakeDisplacement, bd,
                                                    MU, aU, bU, initialWakeAngle, cos_spread, keCorrCT,
                                                    Region2CT, keCorrArray, useWakeAngle,
                                                    adjustInitialWakeDiamToYaw, axialIndProvided, useaUbU, wsPositionXYZw,
                                                    shearCoefficientAlpha, shearZh)

    return wtVelocity, wakeCentersYT, wakeCentersZT, wakeDiametersT, wakeOverlapTRel

def call_floris(turbineX, turbineY, turbineZ, rotorDiameter,\
 ratedPower, windDirections, windSpeeds, windFrequencies, shearExp):

    nTurbines = len(turbineX)
    nDirections = len(windDirections)

    for i in range(nDirections):
        turbineXw, turbineYw = WindFrame(windDirections[i], turbineX, turbineY)
        Vinf = PowWind(windSpeeds[i], turbineZ, shearExp)

    return nTurbines, nDirections, turbineXw, turbineYw, Vinf
```

B.2 Generating wind distributions

```

```

```
3
4  import numpy as np
5  from akima import Akima, akima_interp
6
7  """ Data from a wind rose and directionally averaged wind speed is used to
       create a probability density function for wind direction. This allows
     us to draw samples for calculating the statistics, mean power and
     variance as they are functions of wind direction which is a random
     variable. """
8
9  def denverRose(nDirections):
10
11     # directionally averaged wind speeds
12     windSpeeds=np.array([...]) # array
13
14     # wind direction likelihood from wind rose
15     likelihood=np.array([...]) # array
16
17     # normalize likelihood so that total probability is 1
18     windFrequencies=likelihood/np.sum(likelihood)
19
20     # range of possible wind directions
21     windDirections=np.linspace(0.,360.-360./float(len(windSpeeds)), len(
     windSpeeds))
22
23     # Akima splines to create wind frequency and wind speed functions of
     wind direction
24     spline_freq=Akima(windDirections, windFrequencies)
25     spline_speed=Akima(windDirections, windSpeeds)
26     num=nDirections
27     dirs=np.linspace(0.,360.-360./float(num), num)
28     ddir=dirs[1]-dirs[0]
29
30     frequencies=np.zeros(num)
31     speeds=np.zeros(num)
32
```

```
    # 1000 initial samples to ensure smooth distribution (probability density functions)
    num_int = 1000

    # wind speed distribution
    dir_int1 = np.linspace(dirs[0],dirs[0]+ddir/2.,num_int/2)
    freq_int1 = np.zeros(num_int/2)
    speed_freq_int1 = np.zeros(num_int/2)
    for j in range(num_int/2):
        freq_int1[j],_,_,_ = spline_freq.interp(dir_int1[j])
        ws,_,_,_ = spline_speed.interp(dir_int1[j])
        speed_freq_int1[j] = freq_int1[j]*ws

    # frequency distribution
    dir_int2 = np.linspace(dirs[0],dirs[0]+ddir/2.,num_int/2)
    freq_int2 = np.zeros(num_int/2)
    speed_freq_int2 = np.zeros(num_int/2)
    for j in range(num_int/2):
        freq_int2[j],_,_,_ = spline_freq.interp(dir_int2[j])
        ws,_,_,_ = spline_speed.interp(dir_int2[j])
        speed_freq_int2[j] = freq_int2[j]*ws

    frequencies[0] = np.trapz(freq_int1,dir_int1)+np.trapz(freq_int2,dir_int2)
    speeds[0] = (np.trapz(speed_freq_int1,dir_int1)+np.trapz(speed_freq_int2,dir_int2))/\
        (np.trapz(freq_int1,dir_int1)+np.trapz(freq_int2,dir_int2))

    for i in range(1,num):
        dir_int = np.linspace(dirs[i]-ddir/2.,dirs[i]+ddir/2.,num_int)
        freq_int = np.zeros(num_int)
        speed_freq_int = np.zeros(num_int)
        for j in range(num_int):
            freq_int[j],_,_,_ = spline_freq.interp(dir_int[j])
            ws,_,_,_ = spline_speed.interp(dir_int[j])
            speed_freq_int[j] = freq_int[j]*ws
```

```
        frequencies[i] = np.trapz(freq_int,dir_int)
        speeds[i] = np.trapz(speed_freq_int,dir_int)/np.trapz(freq_int,
    dir_int)

    frequencies = frequencies/sum(frequencies)
    for i in range(len(frequencies)):
        if speeds[i] < 0.:
            speeds[i] = 0.
        if frequencies[i] < 0.:
            frequencies[i] = 0.

    # returns damples wind directions, frequencies, and speed for a given
    sample size
    return dirs, frequencies, speeds
```

B.3 Power calculation

```

import numpy as np
import _floris
from scipy.interpolate import CubicSpline
from scipy import integrate
import scipy


def WindFrame(wind_direction, turbineX, turbineY):
    """ Calculates the locations of each turbine in the wind direction
    reference frame """
    nTurbines = len(turbineX)
    windDirectionDeg = wind_direction
    # adjust directions
    windDirectionDeg = 270. - windDirectionDeg
    if windDirectionDeg < 0.:
        windDirectionDeg += 360.
    windDirectionRad = np.pi*windDirectionDeg/180.0    # inflow wind
    direction in radians
```

```
18
19      # convert to downwind(x)-crosswind(y) coordinates
20      turbineXw = turbineX*np.cos(-windDirectionRad)-turbineY*np.sin(-
    windDirectionRad)
21      turbineYw = turbineX*np.sin(-windDirectionRad)+turbineY*np.cos(-
    windDirectionRad)
22
23      return turbineXw, turbineYw
24
25
26  def PowWind(Uref, turbineZ, shearExp, zref=50., z0=0.):
27      """
28      wind shear power law
29      """
30      nTurbines = len(turbineZ)
31
32      turbineSpeeds = np.zeros(nTurbines)
33
34      for turbine_id in range(nTurbines):
35          turbineSpeeds[turbine_id]= Uref*((turbineZ[turbine_id]-z0)/(zref-
    z0))**shearExp
36
37      return turbineSpeeds
38
39  def WindDirectionPower(rotorDiameter,ratedPower,wtVelocity,Cp=False,\
40  generatorEfficiency=False,cut_in_speed=False,air_density=1.1716):
41      """calculate power from a given wind direction"""
42
43      nTurbines = len(rotorDiameter)
44      if Cp == False:
45          # power coefficient
46          Cp = np.zeros(nTurbines)+0.7737 * 4.0 * 1.0/3.0 * np.power((1. -
    1.0/3.0), 2)
47      if generatorEfficiency == False:
48          generatorEfficiency = np.ones(nTurbines) * 0.93
49      if cut_in_speed == False:
```

```
        cut_in_speed = np.ones(nTurbines)*3.

    rotorArea = 0.25*np.pi*np.power(rotorDiameter, 2)
    # calculate initial values for wtPower (W)
    wtPower = np.zeros(nTurbines)
    for i in range(nTurbines):
        wtPower[i] = generatorEfficiency[i]*\
        (0.5*air_density*rotorArea[i]*Cp[i]*np.power((wtVelocity[i]), 3))
# adjust units from W to kW

    wtPower /= 1000.0

    if np.any(wtPower) >= (np.any(ratedPower)-100.):
        for i in range(0, nTurbines):
            if (ratedPower[i]-100.) <= wtPower[i] <= (ratedPower[i]+100.):
                x = np.array([(ratedPower[i]-100.),ratedPower[i],(
  ratedPower[i]+100.)])
                y = np.array([(ratedPower[i]-100.),ratedPower[i]-25.,
  ratedPower[i]])
                cs = CubicSpline(x,y)
                power = wtPower[i]
                wtPower[i] = cs(power)

            elif wtPower[i] > (ratedPower[i]+100.):
                wtPower[i] = ratedPower[i]

    for i in range(nTurbines):
        if wtVelocity[i] < cut_in_speed[i]:
            wtPower[i] = 0.

    # calculate total power for this direction
    dir_power = np.sum(wtPower)

    # pass out results
    return wtPower, dir_power

```

```
84
85 def power_call(dirs):
86     """ total farm power from each wind direction """
87
88     nTurbines, nDirections, turbineXw, turbineYw, Vinf = \
89     call_floris(turbineX, turbineY, turbineZ, rotorDiameter, ratedPower,
90                                                                 dirs,
    windSpeeds, windFrequencies, shearExp)
91     wtVelocity,_,_,_,_ = Floris(turbineXw, turbineYw, turbineZ,
    rotorDiameter, Vinf)
92
93     dir_powers = np.zeros(nDirections)
94     _,dir_powers[i] = WindDirectionPower(rotorDiameter,ratedPower,
    wtVelocity)
95
96     return dir_powers
```

B.4 Mean power and variance calculation

```
1
2
3 def optVariance(turbineX, turbineY, turbineZ, rotorDiameter, ratedPower,\
4  windDirections, windSpeeds, windFrequencies, shearExp):
5     """ Variance and mean power calculations using the rectangle rule"""
6
7     nTurbines = len(turbineX)
8     nDirections = len(windDirections)
9
10    dir_powers = np.zeros(nDirections)
11    for i in range(nDirections):
12        turbineXw, turbineYw = WindFrame(windDirections[i], turbineX,
    turbineY)
13        Vinf = PowWind(windSpeeds[i], turbineZ, shearExp)
14        wtVelocity,_,_,_,_ = Floris(turbineXw, turbineYw, turbineZ,
    rotorDiameter, Vinf)
```

```
        _,dir_powers[i] = WindDirectionPower(rotorDiameter,ratedPower,
    wtVelocity)

    meanPower = 0.
    varPower = 0.

    for i in range(nDirections):
        meanPower += windFrequencies[i] * dir_powers[i]

    for i in range(nDirections):
        # varPower += windFrequencies[i] * np.abs((dir_powers[i] -
    meanPower))**2
        varPower += windFrequencies[i] * dir_powers[i]**2

    varPower = varPower - meanPower**2

    return meanPower, varPower
```

REFERENCES

[1] S Padrón, A., P J Stanley, A., Thomas, J., J Alonso, J., and Ning, A., 2019. "Polynomial chaos for the computation of annual energy production in wind farm layout optimization." *Journal of Physics: Conference Series,* **753**, 04. 3, 8

[2] Jensen, N., 1983. *A note on wind generator interaction*. 4, 12

[3] Ainslie, J. F., 1988. "Calculating the flowfield in the wake of wind turbines.". 4

[4] Katic, I., Højstrup, J., and Jensen, N., 1987. "A simple model for cluster efficiency." In *EWEC'86. Proceedings. Vol. 1*, W. Palz and E. Sesto, eds., A. Raguzzi, pp. 407–410. 4

[5] Larsen, G., Aa, H., Madsen, F., Bingöl, J., Mann, S., Ott, J., Sørensen, V., Okulov, N., Troldborg, M., Nielsen, K., Thomsen, T., Larsen, R., and Mikkelsen, T., 2007. "Dynamic wake meandering modeling.". 4

[6] Barthelmie, R., Murray, F., and Pryor, S., 2008. "The economic benefit of short-term forecasting for wind energy in the uk electricity market." *Energy Policy,* **36**(5), pp. 1687 – 1696. 4

[7] Orwig, K. D., Ahlstrom, M. L., Banunarayanan, V., Sharp, J., Wilczak, J. M., Freedman, J., Haupt, S. E., Cline, J., Bartholomy, O., Hamann, H. F., Hodge, B., Finley, C., Nakafuji, D., Peterson, J. L., Maggio, D., and Marquis, M., 2015. "Recent trends in variable generation forecasting and its value to the power system." *IEEE Transactions on Sustainable Energy,* **6**(3), July, pp. 924–933. 4

[8] Yu, L., Zhong, S., Bian, X., and Heilman, W. E., 2015. "Temporal and spatial variability of wind resources in the united states as derived from the climate forecast system reanalysis." *Journal of Climate,* **28**(3), pp. 1166–1183. 5

[9] Torralba, V., Doblas-Reyes, F. J., MacLeod, D., Christel, I., and Davis, M., 2017. "Seasonal climate prediction: A new source of information for the management of wind energy resources." *Journal of Applied Meteorology and Climatology,* **56**(5), pp. 1231–1247. 5

[10] Methaprayoon, K., Lee, W., Yingvivatanapong, C., and Liao, J., 2005. "An integration of ann wind power estimation into uc considering the forecasting uncertainty." pp. 116 – 124. 5

[11] Kaminsky, F., Kirchhoff, R., and Sheu, L., 1987. "Optimal spacing of wind turbines in a wind energy power plant." *Solar Energy - SOLAR ENERG,* **39**, 12, pp. 467–471. 6

[12] Hrafnkelsson, B., Oddsson, G., and Unnthorsson, R., 2016. "A method for estimating annual energy production using monte carlo wind speed simulation." *Energies,* **9**, 04, p. 286. 6

[13] Aghabi Rivas, R., Clausen, J., Hansen, K. S., and Jensen, L., 2009. "Solving the turbine positioning problem for large offshore wind farms by simulated annealing." *Wind Engineering,* **33**, 05, pp. 287–297. 6

[14] Attias, K., and Ladany, S., 2006. "Optimal econoimc layout of turbines on windfarms." *Wind Engineering,* **30**, 03, pp. 141–151. 6

[15] Ozturk, U. A., and Norman, B., 2004. "Heuristic methods for wind energy conversion system positioning." *Electric Power Systems Research,* **70**, 08, pp. 179–185. 6

[16] Crosby, P., 1987. "Application of a monte carlo optimization technique to a cluster of wind turbines." *Journal of Solar Energy Engineering, Transactions of the ASME,* **109**, 11, pp. 330–336. 6

[17] Marmidis, G., Lazarou, S., and Pyrgioti, E., 2008. "Optimal placement of wind turbines in a wind park using monte carlo simulation." *Renewable Energy,* **33**, 07, pp. 1455–1460. 6

[18] Grady, S., Hussaini, M., and Abdullah, M., 2005. "Placement of wind turbines using genetic algorithms." *Renewable Energy,* **30**, 02, pp. 259–270. 6

[19] Thomas, J., and Ning, A., 2018. "A method for reducing multi-modality in the wind farm layout optimization problem." *Journal of Physics: Conference Series,* **1037**, 06, p. 042012. 6, 7

[20] L. Du Pont, B., and Cagan, J., 2010. "An extended pattern search approach to wind farm layout optimization." Vol. 134. 6

[21] Adewunmi, A., and Aickelin, U., 2012. "Investigating the effectiveness of variance reduction techniques in manufacturing, call center and cross-docking discrete event simulation models." *SSRN Electronic Journal*, 04. 7

[22] Owen, A. B., 2013. *Monte Carlo theory, methods and examples*. 7, 33

[23] Chaudhuri, S., Das, G., Datar, M., Motwani, R., and Narasayya, V., 2001. "Overcoming limitations of sampling for aggregation queries." pp. 534 – 542. 7

[24] Simpson, T., and Lin, D., 2001. "Sampling strategies for computer experiments: Design and analysis." *Int. J. Reliab. Appl.,* **2**, 01. 7

[25] Borissova, D., and Mustakerov, I., 2017. "Designing of wind farm layout by using of multi-objective optimization." *International Journal of Mathematical Models and Methods in Applied Sciences,* **11**, 01, pp. 290–295. 8

[26] Mytilinou, V., and Kolios, A., 2017. "A multi-objective optimisation approach applied to offshore wind farm location selection." *Journal of Ocean Engineering and Marine Energy,* **3**, 07. 8

[27] Feng, J., and Shen, W. Z., 2015. "Modelling wind for wind farm layout optimization using joint distribution of wind speed and wind direction." *Energies,* **8**, 04, pp. 3075–3092. 8

[28] Foti, D., Yang, X., and Sotiropoulos, F., 2016. "Uncertainty quantification of infinite aligned wind farm performance using non-intrusive polynomial chaos and a distributed roughness model: Uncertainty quantification of infinite aligned wind farm performance." *Wind Energy,* **20**, 12. 8

[29] Tingey, E., Thomas, J., and Ning, A., 2015. "Wind farm layout optimization using sound pressure level constraints." pp. 154–159. 9

[30] Gebraad, P., W. Teeuwisse, F., Wingerden, J. W., Fleming, P., D. Ruben, S., Marden, J., and Pao, L., 2014. "Wind plant power optimization through yaw control using a parametric model for wake effects—a cfd simulation study." *Wind Energy*, 12. 12, 13

[31] Akima, H., 1970. "A new method of interpolation and smooth curve fitting based on local procedures." *J. ACM,* **17**, 10, pp. 589–602. 15

[32] Marler, R., and Arora, J., 2004. "Survey of multi-objective optimization methods for engineering." *Structural and Multidisciplinary Optimization,* **26**, 04, pp. 369–395. 17, 18, 19

[33] Pareto, V., 1971 (1906). *Manual of political economy (manuale di economia politica)*. Kelley, New York Translated by Ann S. Schwier and Alfred N. Page. 17, 18

[34] Chang, K.-H., 2015. "Chapter 19 - multiobjective optimization and advanced topics." In *e-Design*, K.-H. Chang, ed. Academic Press, Boston, pp. 1105 – 1173. 19

[35] Perez, R. E., Jansen, P. W., and Martins, J. R. R. A., 2012. "pyOpt: A Python-based object-oriented framework for nonlinear constrained optimization." *Structural and Multidisciplinary Optimization,* **45**(1), January, pp. 101–118. 22

[36] Gill, P., Murray, W., and Saunders, M., 2002. "Snopt: An sqp algorithm for large-scale constrained optimization." *SIAM Journal on Optimization,* **12**, 04, pp. 979–1006. 22